Progress Report No. 1

on

Contract NASw-835

Amendment No. 4

for period

1 October 1964 - 31 March 1965

Prepared for

National Aeronautics and Space Administration
Washington, D. C.

ELECTROMAGNETIC RESEARCH CORPORATION
5001 COLLEGE AVENUE
COLLEGE PARK, MD.

PROGRESS REPORT NO. 1

on

Contract NASw-835
Amendment No. 4

1. INTRODUCTION

Contract NASw-835 supports studies related to ionospheric probing. The basic contract calls for a program of theoretical studies, which were carried out during the period 1 October 1963 - 1 October 1964. Amendment 4 provides for a continuation of these theoretical studies for an additional year.

Amendment 4 encompasses four principal tasks, as follows:

1) Current distribution, field patterns, and impedance of long antennas in the ionosphere.

2) Effects of finite thermal velocities of the charged particles in the ionosphere on antenna properties.

3) Effects of ion sheaths around antennas on their radiation properties in the ionosphere.

4) Nonlinear effects of electron motion on antenna radiation from the standpoint of diagnostics.

The topics covered in this report are items 1), 2) and 4) above. Note that the discussion of item 2) is included with that of item 4). It is planned to reactivate work on item 3) during the next quarter.

Due to the late date on which Amendment 4 was issued, the present report covers the six-month period 1 October 1964 - 31 March 1965. It thus combines the material that normally would have appeared in two separate quarterly progress reports.

2. CURRENT DISTRIBUTION, DIRECTIVE PATTERNS, AND IMPEDANCE OF ANTENNAS

The work program carried out under the assignment of task 1) is discussed in the following section.

2.1 CURRENT DISTRIBUTION

As an outgrowth of the analysis of the impedance of a dipole antenna, the variational technique was applied to optimize the propagation constant for the current along the dipole. This technique is discussed in detail in Scientific Report No. 1 (to be referred to as SR 1 hereafter). Although the variational technique is capable of optimizing the parameters in an assumed functional form for the current distribution, it cannot determine whether the assumed functional form is accurate. For this, one must determine how closely the boundary conditions at the surface of the antenna are satisfied. In particular, the usual assumption of a sinusoidal form may not be sufficiently accurate for long antennas.

The limiting case of a long antenna is one of infinite length. This is actually simpler to handle mathematically, since end effects disappear. Thus the case of an infinite, perfectly conducting wire has been selected for initial study. The wire, of radius a, is oriented at an arbitrary angle θ with respect to the terrestrial magnetic field H_0, which is in the z-direction.

As in the dipole impedance analysis, two rectangular coordinate systems are used, $\Sigma(x,y,z)$ and $\Sigma'(x',y',z')$, (see Fig. 1), where z is along $\underset{\sim}{H}_0$ and where z' along the axis of the cylinder. The x and x' axis coincide, so that the axis of the cylinder is in the yz-plane.

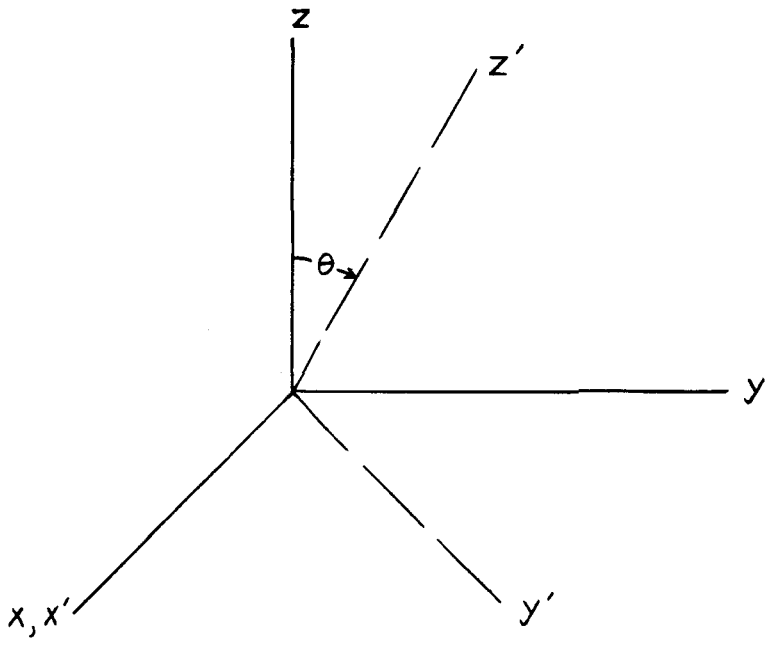

Fig. 1

The electric field, $\underset{\sim}{E}(x)$, is given in terms of a Green's function representation by

$$\underset{\sim}{E}(\underset{\sim}{x}) = \int d^3x_1 \cdot \underset{\sim}{G}(\underset{\sim}{x}-\underset{\sim}{x}_1) \cdot \underset{\sim}{J}(\underset{\sim}{x}_1) \tag{1}$$

where $\underset{\sim}{x}$ is the position of the field point and $\underset{\sim}{x}_1$ that of the source, and $\underset{\sim}{J}(\underset{\sim}{x}_1)$ is the surface current density.

With the above representation for $\underset{\sim}{E}(\underset{\sim}{x})$, integral equations for $\underset{\sim}{J}(\underset{\sim}{x})$ may be determined from the boundary conditions on the surface of the cylinder, which are the vanishing points of the tangential components of $\underset{\sim}{E}(\underset{\sim}{x})$ at the surface of the cylinder. Hence

$$n' \times \underset{\sim}{E}(\underset{\sim}{x})\Big]_{r'=a} = \int d^3x_1 \, n' \times \underset{\sim}{G}(\underset{\sim}{x}-\underset{\sim}{x}_1) \cdot \underset{\sim}{J}(\underset{\sim}{x}_1)\Big]_{r'=a} \tag{2}$$

where $\underset{\sim}{n}'$ is the unit normal to the cylinder and r' is the radial variable of the

cylindrical coordinates r', ϕ', z' in the Σ' system. Since $\underset{\sim}{J}(\underset{\sim}{x}_1)$ is a surface current density, it may be represented as the sum of vectors in the z', and ϕ' directions,

$$\underset{\sim}{J}(\underset{\sim}{x}_1) = J_1(\underset{\sim}{x}_1)\hat{e}_{z'} + J_2(\underset{\sim}{x})\hat{e}_{\phi'} \tag{3}$$

Hence (2) represents a system of linear homogeneous integral equations in J_1 and J_2.

Since the integral equations (2) are not readily solvable by known techniques as long as $J_1(\underset{\sim}{x})$ and $J_2(\underset{\sim}{x})$ are completely arbitrary, we are led to making assumptions as to functional forms for J_1 and J_2. We assume that

$$J_1(\underset{\sim}{x}_1) = e^{ikz'} \sum_{n=-\infty}^{\infty} a_n e^{in\phi'} , \tag{4}$$

$$J_2(\underset{\sim}{x}_1) = e^{ikz'} \sum_{n=-\infty}^{\infty} b_n e^{in\phi'} , \tag{5}$$

where the Fourier series $\sum_{-\infty}^{\infty} a_n e^{in\phi'}$ and $\sum_{-\infty}^{\infty} b_n e^{in\phi'}$ represent arbitrary ϕ' dependence, whose coefficients are to be determined. K is the propagation constant, which also is to be determined.

After substituting (4) and (5) into (2), it may be shown that the tangential components of $\underset{\sim}{E}$ have the form $e^{ikz'}$ multiplied by a function of ϕ', the Fourier coefficients a_n, b_n, the radius a and the propagation constant K. That is,

$$E_{z'}\Big|_{cylinder} = e^{ikz'} f(a, a_n, b_n, K, \phi') = 0 \tag{6}$$

and

$$E_{\phi'}\Big|_{cylinder} = e^{ikz'} g(a, a_n, b_n, K, \phi') = 0 \tag{7}$$

The constants a_n, b_n and K must be determined so that f and g are identically zero. To do this we expand f and g in Fourier series

$$f = \sum_{n=-\infty}^{\infty} c_n(a, a_m, b_m, K) e^{in\phi'} \tag{8}$$

$$g = \sum_{n=-\infty}^{\infty} d_n(a, a_m, b_m, K) e^{in\phi'} \tag{9}$$

By uniqueness of Fourier series, we have the set of equations

$$c_n(a, a_m, b_m, K) = 0 \tag{10}$$

$$d_n(a, a_m, b_m, K) = 0 \tag{11}$$

to determine a_m, b_m and K. To simplify (10) and (11), only the leading order term in the small parameter a will be retained.

2.2 DIRECTIVE PATTERN

The directive pattern of an antenna is the relative variation of the far field with the angular coordinates about the antenna. The far field is that at a distance which is very large compared to the dimensions of the current distribution and the wavelength. Consequently, the current distribution, for a given direction, is "seen" from the field point as a localized source. Thus the essential information regarding the properties of the far field can be determined by investigating the far field of a point source. For any other current distribution, this result can be integrated over the current distribution to obtain the radiation pattern of the finite source. This last integration presents no difficulty.

A rather general treatment of the far field problem for a homogeneous cold collisionless ionosphere was given by Arbel and Felsen [1]. The far field properties depend heavily on the dispersion curve, which is determined by the normalized ionosphere parameters X and Y. Arbel and Felsen divided the positive

XY-plane into 9 regions, each giving rise to a different form of dispersion curve. Actually, however, there are 14 distinct regions, as discussed sometime earlier by Clemmow and Mullaly [2]. Thus, the Arbel-Felsen treatment is incomplete. In particular, for certain cases where the wave frequency is well below the plasma and gyro frequencies, multiple paths are possible. Since this situation appears to be of importance to satellite radio astronomy, we shall discuss it in detail.

First, the 14 classes of dispersion curves will be discussed, and then the determination of the far field for the VLF situation mentioned above will be carried out. The Arbel-Felsen treatment is extended by including a small normalized collision frequency, since this is found to eliminate a singularity of the field due to a point source. The procedure presented includes that to be followed in the general case.

2.2.1 Analysis of Dispersion Curve

In determining the far field from a point source, Green's function representation (1) is used for the electric field $E(\underset{\sim}{x})$, where

$$G(\underset{\sim}{x}-\underset{\sim}{x}') = \int d^3q \, \frac{N}{D} \, e^{-i\underset{\sim}{q}\cdot(\underset{\sim}{x}-\underset{\sim}{x}')} \quad . \tag{12}$$

The matrix N is familiar from the impedance analysis. D, expressed in cylindrical coordinates σ, p, where σ is the coordinate parallel to the direction of the magnetic field and p is the radial coordinate normal to the direction of the magnetic field, is given by

$$D = -\alpha_3\sigma^4 + \sigma^2\left\{p^2(-\alpha_1-\alpha_3)+2\alpha_1\alpha_3\right\} + \left\{-\alpha_1 p^4 + p^2(\alpha_1^2-\alpha_3^2+\alpha_1\alpha_3) - \alpha_3(\alpha_1^2-\alpha_2^2)\right\} . \tag{13}$$

Of particular interest in the far field calculation are the roots of D = 0 in the collisionless case, that is, when the parameters α_1, α_2, α_3 are real. These parameters are then expressed in terms of the normalized plasma and gyro frequency parameters X and Y through

$$\begin{aligned} \bar{\alpha}_1 &= 1 - \frac{X}{1-Y^2} \\ \bar{\alpha}_2 &= \frac{XY}{1-Y^2} \\ \bar{\alpha}_3 &= 1-X \end{aligned} \tag{14}$$

where a bar is used over α_1, α_2, α_3 to indicate the collisionless case. The roots σ_1^2, σ_2^2 of D = 0 in terms of p are then

$$\begin{aligned} \sigma_{1,2}^2 &= \frac{p^2(\bar{\alpha}_1+\bar{\alpha}_3)-2\bar{\alpha}_1\bar{\alpha}_3}{2\bar{\alpha}_3} \pm \frac{1}{2\bar{\alpha}_3}\sqrt{\left[p^2(\bar{\alpha}_1+\bar{\alpha}_3)-2\bar{\alpha}_1\bar{\alpha}_3\right]^2 - 4\bar{\alpha}_1\bar{\alpha}_3\left(p^2-\bar{\alpha}_3\right)\left(p^2\frac{\bar{\alpha}_1^2-\bar{\alpha}_2^2}{\bar{\alpha}_1}\right)} \\ &= \frac{p^2(\bar{\alpha}_1+\bar{\alpha}_3)-2\bar{\alpha}_1\bar{\alpha}_3}{2\bar{\alpha}_3} \pm \frac{1}{2\bar{\alpha}_3}\sqrt{p^4(\bar{\alpha}_1-\bar{\alpha}_3)^2 - 4p^2\bar{\alpha}_3\bar{\alpha}_2^2 + 4\bar{\alpha}_3^2\bar{\alpha}_2^2} \\ &\equiv \frac{1}{2\bar{\alpha}_3}\left(U \pm \sqrt{U^2+W}\right) \quad . \end{aligned} \tag{15}$$

Depending on the relative values of X and Y, σ_1^2 and σ_2^2 may be positive and real, negative and real, or complex. We are specifically interested in the positive real values of σ_1^2 and σ_2^2, for positive values of p^2 so that σ_1 and σ_2 may be real. In the collisionless case, the real values of σ_1 and σ_2 determine the propagating waves in the medium. Likewise we are interested in the shape of the curves σ_1, σ_2 plotted versus p, since these will determine the stationary ray paths. Of particular interest is the position of relative maxima and minima, turning points of the curve, i.e., points for which

$$\frac{d^2\sigma_i}{dp^2} = 0 \tag{16}$$

and double turning points, i.e., points for which

$$\frac{d^2\sigma_i}{dp^2} = \frac{d^3\sigma_i}{dp^3} = 0 \ . \tag{17}$$

The real values of σ_1 and σ_2 are determined by considering the signs and the relative magnitude of the quantities U and W, in (15) which are given by

$$U = p^2(\bar{\alpha}_1 + \bar{\alpha}_3) - 2\bar{\alpha}_1\bar{\alpha}_3 \tag{18}$$

and

$$W = -4\bar{\alpha}_3\bar{\alpha}_1\left(p^2 - \bar{\alpha}_3\right)\left(p^2 - \frac{\bar{\alpha}_1^2 - \bar{\alpha}_2^2}{\bar{\alpha}_1}\right) . \tag{19}$$

The sign of W depends on the sign of $\bar{\alpha}_3$, $\bar{\alpha}_1$, the relative magnitudes of $\bar{\alpha}_3$ and $\frac{\bar{\alpha}_1^2 - \bar{\alpha}_2^2}{\bar{\alpha}_1}$ and the value of p^2 with respect to the last two quantities. Of concern are the relative magnitudes of U^2 and W in a region of the X, Y plane where

$$U^2 + W = p^4(\bar{\alpha}_1 - \bar{\alpha}_3)^2 + p^2\left(-4\bar{\alpha}_2^2\bar{\alpha}_3\right) + 4\bar{\alpha}_3^2\bar{\alpha}_2^2 = 0 \tag{20}$$

[see (16)].

In [1] the first quadrant of the X, Y plane is divided into nine regions. The dispersion curve in each region differs from that in adjacent regions by whether or not one, both, or none of the roots, σ_1, σ_2 are real and whether or not

σ_1 and σ_2 have unbounded real values. The graph of the X, Y plane divided into the 9 regions is given in Fig. 2, accompanied by the inequalities which determine the regions.

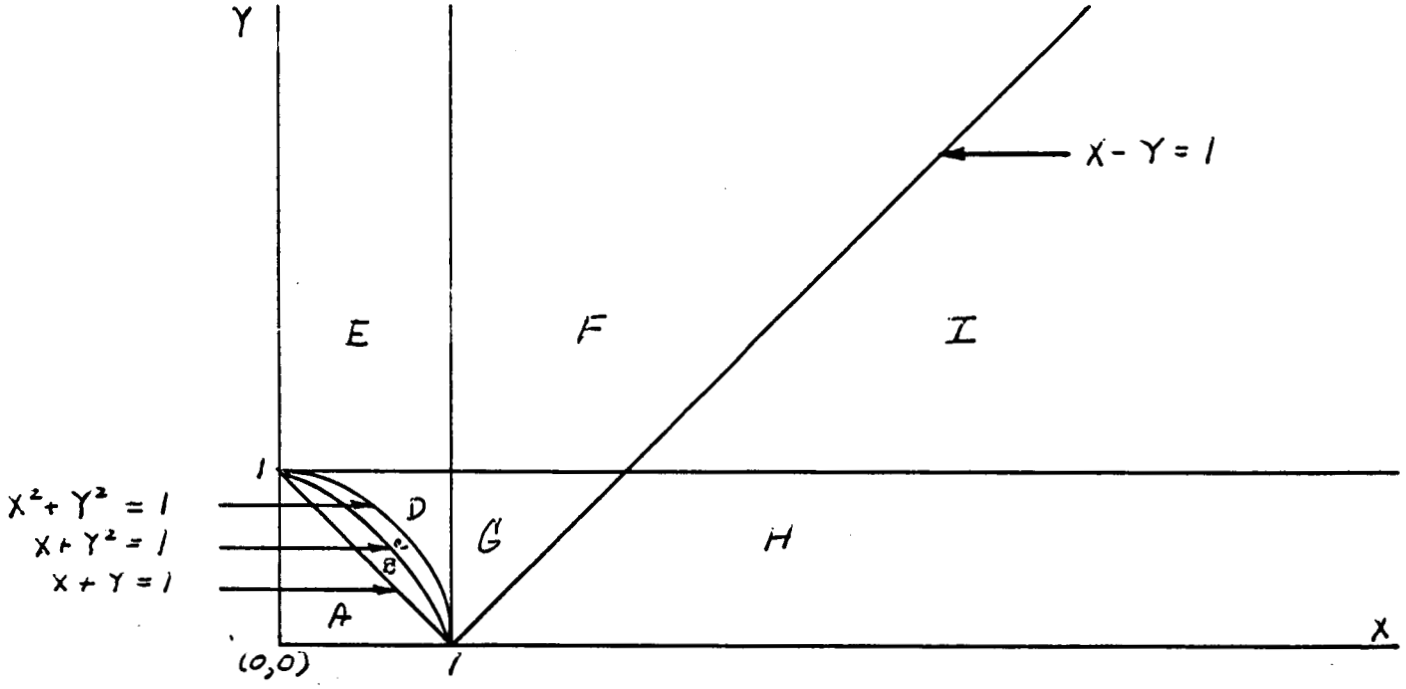

FIG. 2

Region A: $1 > X + Y$

Region B: $X + Y > 1 > X + Y^2$

Region C: $X + Y^2 > 1 > X^2 + Y^2$

Region D: $X^2 + Y^2 > 1 > \max [Y, X]$

Region E: $Y > 1 > X$

Region F: $\min (Y, X) > 1 > X - Y$

Region G: $X > 1 > \max [Y, X - Y]$

Region H: $X - Y > 1 > Y$

Region I: $\min [Y, X - Y] > 1$

In the calculation of the far field due to a point source, it is necessary to know when the curves of σ_1, σ_2 versus p possess turning points (points of inflection), that is, the points for which

$$\frac{d^2\sigma_i}{dp^2} = 0.$$

It is also necessary to determine the double turning points for which

$$\frac{d^2\sigma_i}{dp^2} = \frac{d^3\sigma_i}{dp^3} = 0.$$

In determining these points, we find that some of the regions given above must be subdivided in order that the number and location of the turning points be specified. Fig. 3 shows the X, Y plane with the subregions specified. Inequalities are included when regions differ from those given in Fig. 2.

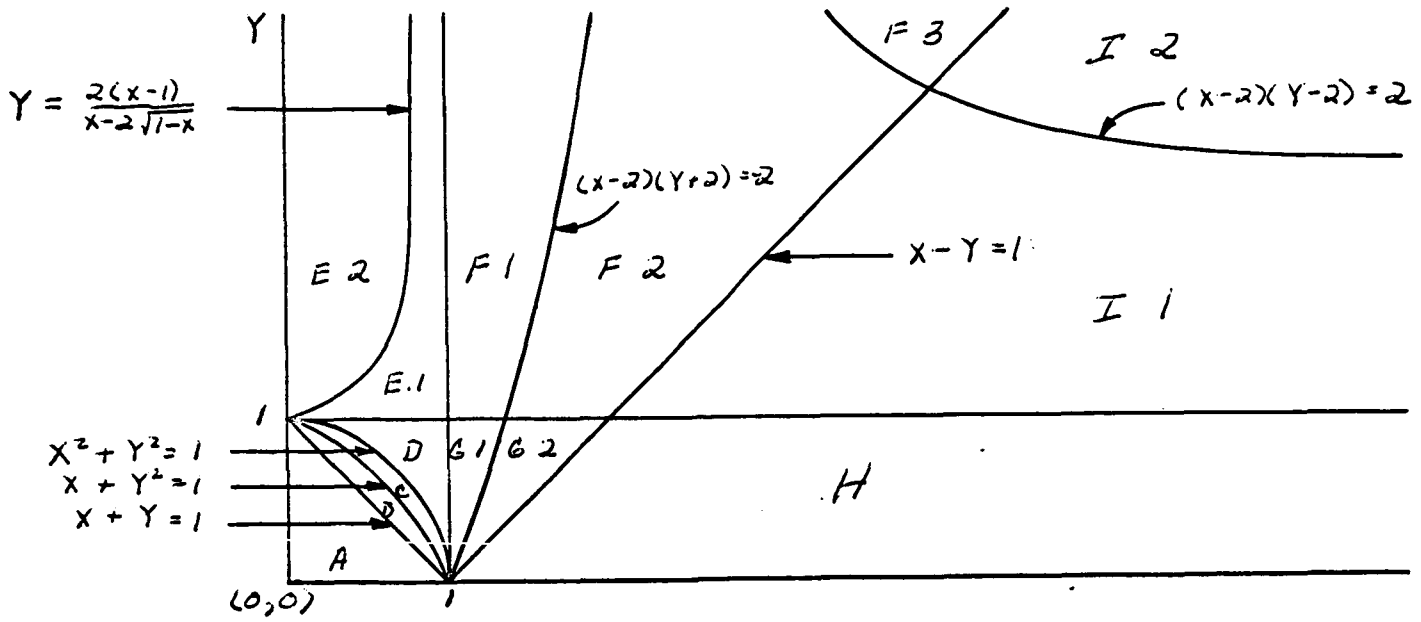

FIG. 3

Region E.1: $$X < i < \min\left[Y,\ X + \frac{Y}{3Y - 2 + 2\sqrt{2Y(Y-1)}} \right]$$

Region E.2: $$\max\left[X,\ X + \frac{Y}{3Y - 2 + 2\sqrt{2Y(Y-1)}} \right] < i < Y$$

Region F.1: $$\frac{2}{(2 - X)(Y + 2)} < i < \min\ (Y,\ X)$$

Region F.2: $$\max\left[X - Y,\ \frac{(X-2)(Y-2)}{2} \right] < i < \min\left[X,\ \frac{2}{(2-X)(Y+2)} \right]$$

Region F.3: $$X - Y < i < \min\left[X, \frac{(X-2)(Y-2)}{2} \right]$$

Region G.1: $$\max\left[Y,\ \frac{2}{(2-X)(Y+2)} \right] < i < X$$

Region G.2: $$\max\left[Y,\ X - Y \right] < i < \min\left[X,\ \frac{2}{(2-X)(Y+2)} \right]$$

Region I.1: $$\frac{(X-2)(Y-2)}{2} < i < \min\left[Y,\ X - Y \right]$$

Region I.2: $$i < \min\left[Y,\ X - Y,\ \frac{(X-2)(Y-2)}{2} \right]$$

Characteristic curves will now be given for each region or subregion. As the curves have some common characteristics, these will be discussed first and then a more complete description for each region will be given. The actual curves are given at the end.

First of all, we note from (15) that the dispersion curves are symmetric with respect to both the σ and p axes; thus, we may frequently confine our discussion to the upper half plane ($\sigma \geq 0$). If the curve intersects the p-axes it does so at either $p = \pm\sqrt{\bar{\alpha}_3}$ or $p = \pm p_2$ where

$$p_2 \simeq \sqrt{\frac{\bar{\alpha}_1^2 - \bar{\alpha}_1^2}{-\bar{\alpha}_1}}\ . \tag{21}$$

If the curve is unbounded it has for asymptotes $\sigma = \pm p\sqrt{-\bar{\alpha}_1/\bar{\alpha}_3}$.

Toward determining maxima and minima of the curves, one differentiates σ_i^2 with respect to p to obtain

$$2\sigma_i \frac{d\sigma_i}{dp} = \frac{-p\left[-4\bar{a}_1 p^2 + 2(\bar{a}_1^2 - \bar{a}_2^2 + \bar{a}_1\bar{a}_3) + 2(-\bar{a}_1 - \bar{a}_3)\sigma_i^2\right]}{\left[-2\bar{a}_3\sigma_i^2 + p^2(-\bar{a}_1 - \bar{a}_3) + 2\bar{a}_1\bar{a}_3\right]}. \tag{12}$$

Thus, $\frac{d\sigma_i}{dp}$ is zero when the numerator of (22) is zero; and upon substitution for σ_i^2 we obtain the points for which there are possible maxima or minima to be

$$p = 0$$

and

$$\bar{p}^2, \bar{\bar{p}}^2 = \frac{2\bar{a}_1\bar{a}_3\bar{a}_2^2 \pm \sqrt{(2\bar{a}_1\bar{a}_3\bar{a}_2^2)^2 - \bar{a}_1\bar{a}_2^2\bar{a}_3(\bar{a}_1 - \bar{a}_3)^2\left[(\bar{a}_1 + \bar{a}_3)^2 - \bar{a}_2^2\right]}}{\bar{a}_1(\bar{a}_1 - \bar{a}_3)^2}. \tag{13}$$

The existence of maxima and minima at these points depends on whether or not $\bar{p}$ and $\bar{\bar{p}}$ are real and whether or not values of σ_i corresponding to $p = 0$, $\bar{p}$, $\bar{\bar{p}}$ are real.

The turning points are determined by three methods. One is by noting the possible maxima and minima. If in a single branch of σ_i, $\sigma_i > 0$, we obtain both relative maxima and minima, a turning point must lie between. This is the case in Regions F 1, F 3, G 1, I 2. Likewise, if we consider p as a function of σ and obtain on a branch both maxima and minima for p as a function of σ, $(p > 0)$, then a turning point must lie between the two extremes. This is the case in Region D. Lastly, turning points may occur without the occurrence of alternating extremes. The method of determining the existence of these turning points is discussed thoroughly in [2]. Briefly, one determines the expression for $\frac{d^2\sigma_1}{dp^2} = 0$ and then seeks to determine for what values of X and Y this equation has a double root. This expression determines the boundary between Region E 1 and Region E 2. It is then readily shown that the turning points separate in Region E 1 for real values of σ_1 and move into the complex plane in Region E 2. We shall not determine the location of the turning points explicitly but for ease of notation will denote them by $p = \pm p', \pm p''$.

The following is the discussion of the dispersion curve in each region or subregion:

Region A: $1 > X + Y$

Here we have bounded curves for σ_1 and σ_2 where σ_1 and σ_2 intersect the p-axis at $p = \pm\sqrt{\bar{\alpha}_3}$ and $p = \pm p_2$, respectively. Both curves have relative maxima at $p = 0$ $(\sigma > 0)$ and neither curve possesses turning points.

Region B: $X + Y > 1 > X + Y^2$

Here we have a curve only for σ_1 and the curve is bounded. It intersects the p-axis at $p = \pm\sqrt{\bar{\alpha}_3}$, has a relative maximum at $p = 0$, and has no turning points.

Region C: $X + Y^2 > 1 > X^2 + Y^2$

Here we have a curve only for σ_1. There is a bounded branch intersecting the p-axis at $p = \pm\sqrt{\bar{\alpha}_3}$, having a relative maximum at $p = 0$ $(\sigma > 0)$, and possessing no turning points. There is also an unbounded branch intersecting the p-axis at $p = \pm p_2$ and possessing no turning points.

Region D: $X^2 + Y^2 > 1 > \max\,[Y, X]$

Here we have curves for both σ_1 and σ_2. There is a bounded branch for σ_1 intersecting the p-axis at $p = \pm\sqrt{\bar{\alpha}_3}$, having a relative maximum at $p = 0$ $(\sigma > 0)$, and possessing no turning points. There is an unbounded branch for σ_1 intersecting neither axis, having no turning points, and existing for $\infty > p > p_4$, $-\infty < p < -p_4$ where

$$p_4^2 = \frac{2\bar{\alpha}_3\bar{\alpha}_2^2}{(\bar{\alpha}_1 - \bar{\alpha}_3)^2}\left[1 + \sqrt{1 - \frac{(\bar{\alpha}_1 - \bar{\alpha}_3)^2}{\bar{\alpha}_2^2}}\right].$$

For σ_2 we have a bounded branch intersecting the p-axis at $p = \pm p_2$ and existing for $p_4 \leq p \leq p_2$ and $-p_2 \leq p \leq -p_4$. There are turning points of the curve at $p = \pm p'$.

Region E 1: $$X < 1 < \min\left[Y,\ X + \frac{Y}{3Y - 2 + 2\sqrt{2Y\,(Y-1)}} \right]$$

In this region we have bounded curves for both σ_1 and σ_2. σ_1 intersects the p-axis at $p = \pm\sqrt{\bar{\alpha}_3}$, has no turning points and a relative maximum at $p = 0$ ($\sigma > 0$). σ_2 intersects the p-axis at $p = \pm p_2$ and has a relative maximum at $p = 0$ ($\sigma > 0$); there are two turning points of this curve in each quadrant located at $p = \pm p'$ ' and $p = \pm p''$.

Region E 2: $$\max\left[X,\ X + \frac{Y}{3Y - 2 + 2\sqrt{2Y\,(Y-1)}} \right] < 1 < Y$$

Here we have bounded curves with no turning points for σ_1, σ_2. Each curve has a relative maximum at $p = 0$ ($\sigma > 0$), and σ_1 and σ_2 intersect the p-axis at $p = \pm p_2$ and $p = \pm\sqrt{\bar{\alpha}_3}$, respectively.

It should be noted here that the boundary between Region E 1 and Region E 2 is determined in [2]. At this boundary the turning points coalesce or $p' \to p''$ so that at the boundary

$$\left.\frac{d^2\bar{\sigma}_1}{d\rho^2}\right|_{\rho=\rho''} = \left.\frac{d^3\bar{\sigma}_1}{d\rho^3}\right|_{\rho=\rho''} = 0$$

Region F 1: $$\min\,(Y,\ X) > 1 > \frac{2}{(2-X)(Y+2)}$$

Here we have an unbounded branch for σ_2 and a bounded branch for σ_1. σ_2 has a minimum at $p = 0$ ($\sigma > 0$) and no turning points. σ_1 has a relative minimum at $p = 0$ ($\sigma > 0$) and maxima at $p = \pm\bar{p}$ ($\sigma > 0$). There are turning points for σ_1 in each quadrant at $p = \pm p'$ where $0 \le p' \le \bar{p}$. σ_1 intersects the p-axis at $p = \pm p_2$.

Region F 2: $$\min\left(X,\ \frac{2}{(2-X)(Y+2)}\right) > 1 > \max\left[X - Y,\ \frac{(X-2)(Y-2)}{2} \right]$$

Again we have an unbounded branch for σ_2 and a bounded branch for σ_1. However, in neither branch are there turning points. σ_2 has a relative minimum at $p = 0$ ($\sigma > 0$). σ_1 intersects the p-axis at $p = \pm p_2$ and has a relative maximum at $p = 0$.

It should be noted that at the boundary between the regions F.1 and F.2, that is, where $(2-X)(Y+2) = 1$, $Y > 1$, $\bar{p} \to p' \to 0$ so that at $p = 0$

$$\left.\frac{d\sigma_1}{dp}\right|_{p=0} = \left.\frac{d^2\sigma_1}{dp^2}\right|_{p=0} = \left.\frac{d^3\sigma_1}{dp^3}\right|_{p=0} = 0$$

Otherwise the curve is as in Region F 2.

Region F 3: $\min\left(X, \frac{(X-2)(Y-2)}{2}\right) > 1 > X - Y$

There is an unbounded branch for σ_2 and a bounded branch for σ_1. σ_1 has no turning points; it exists for $-p_2 \le p \le p_2$ and has a maximum at $p = 0$ $(\sigma > 0)$. σ_2 has a relative maximum at $p = 0$ $(\sigma > 0)$, minimums at $p = \pm \bar{p}$ $(\sigma > 0)$, and thus turning points in each quadrant at $p = \pm p'$, $0 \le p' \le \bar{p}$. We note that at the boundary between F 2 and F 3, that is where $(X-2)(Y-2) = 2$ and $X-Y < 1$, $\bar{p} \to p' \to 0$, so that we have at $p = 0$

$$\left.\frac{d\sigma_2}{dp}\right|_{p=0} = \left.\frac{d^2\sigma_2}{dp^2}\right|_{p=0} = \left.\frac{d^3\sigma_2}{dp^3}\right|_{p=0} = 0$$

Region G 1: $\max\left[Y, \frac{2}{(2-X)(Y+2)}\right] < 1 < X$

There is no curve for σ_1 and a bounded curve for σ_2. σ_2 exists for $-p_2 \le p \le p_2$. It has a relative minimum at $p = 0$ $(\sigma > 0)$ and a maximum at $p = \pm \bar{p}$. Thus there is a turning point in each quadrant at $p = \pm p'$, $0 \le p' \le \bar{p}$.

Region G 2: $\max\left[Y, X-Y\right] < 1 < \min\left[X, \frac{2}{(2-X)(Y+2)}\right]$

Again there is no curve for σ_1 and a bounded curve for σ_2. σ_2 exists for $-p_2 \le p \le p_2$, has a maximum at $p = 0$, $(\sigma > 0)$ and no turning points. We note that at the boundary of Region G 1 and G 2, that is, $(X-2)(Y+2) = 2$, $Y < 1$, $\bar{p} \to \bar{p}' \to 0$ so that at $p = 0$

$$\left.\frac{d\sigma_2}{dp}\right|_{p=0} = \left.\frac{d^2\sigma_2}{dp^2}\right|_{p=0} = \left.\frac{d^3\sigma_2}{dp^3}\right|_{p=0} = 0$$

Otherwise the curve is as given in Region G 2.

Region I 1: $\min [Y, X-Y] > 1 > \frac{(X-2)(Y-2)}{2}$

We have no curve for σ_1 and an unbounded branch for σ_2. σ_2 exists for $-\infty \leq p \leq \infty$, does not intersect the p-axis and has a minimum at $p = 0$ $(\sigma > 0)$.

Region I 2: $\min \left[Y, X - Y, \frac{(X-2)(Y-2)}{2}\right] > 1.$

Again there is no curve for σ_1 and an unbounded branch for σ_2. σ_2 exists for $-\infty \leq p \leq \infty$ and does not intersect the p-axis. There is a relative maximum at $p = 0$ $(\sigma > 0)$ and a relative minimum at $p = \pm \bar{p}$ $(\sigma > 0)$; thus, there is a turning point in each quadrant at $p = \pm p'$ where $0 \leq p' \leq \bar{p}$. At the boundary between Region I 1 and Region I 2, that is where $\frac{(X-2)(Y-2)}{2} = 1$ and $X - Y > 1$, $\bar{p} \to p' \to 0$ so that at $p = 0$, we have

$$\left.\frac{d\sigma_1}{dp}\right|_{p=0} = \left.\frac{d^2\sigma_2}{dp^2}\right|_{p=0} = \left.\frac{d^3\sigma_2}{dp^3}\right|_{p=0} = 0,$$

Other properties at the curve are as given in Region I 1.

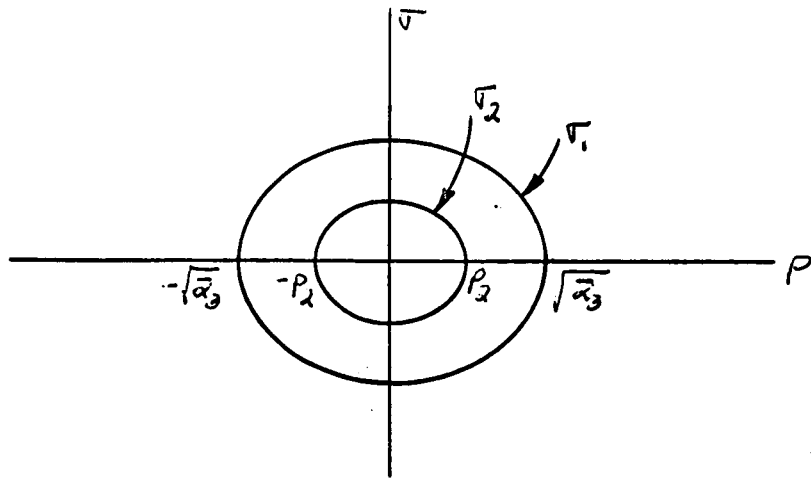

FIG. 4

Region A: $1 > X + Y$

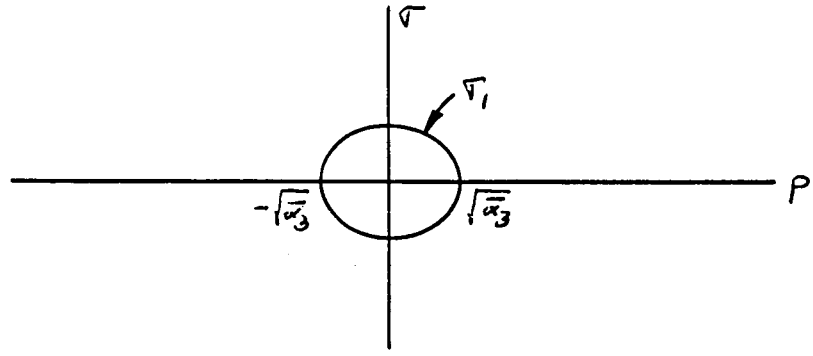

FIG. 5

Region B: $X + Y > 1 > X + Y^2$

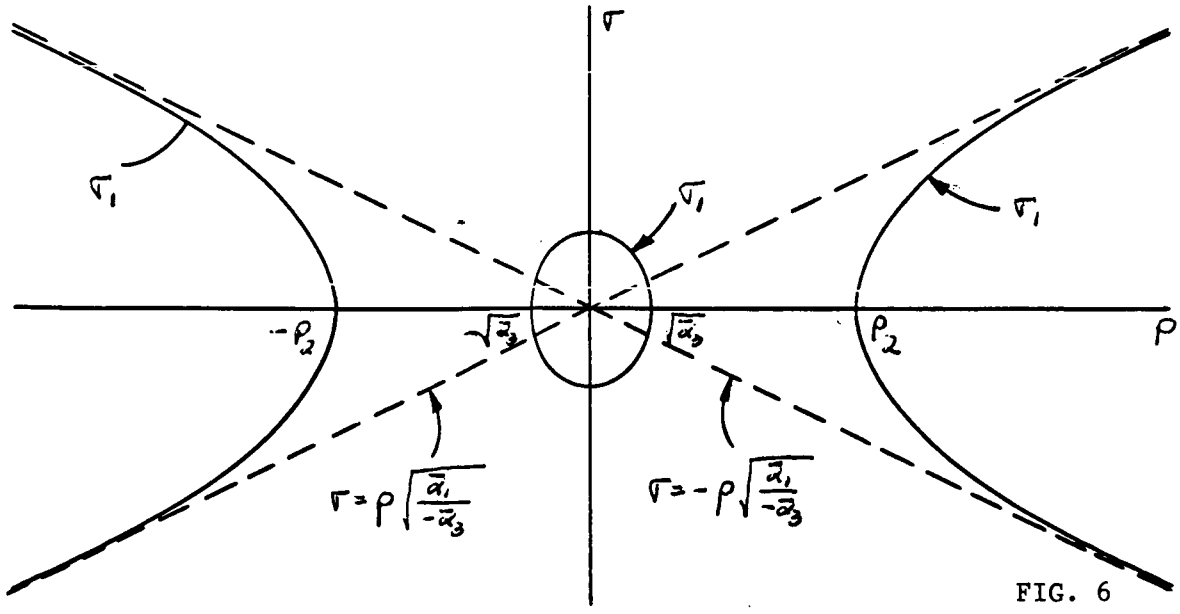

FIG. 6

Region C: $X + Y^2 > 1 > X^2 + Y^2$

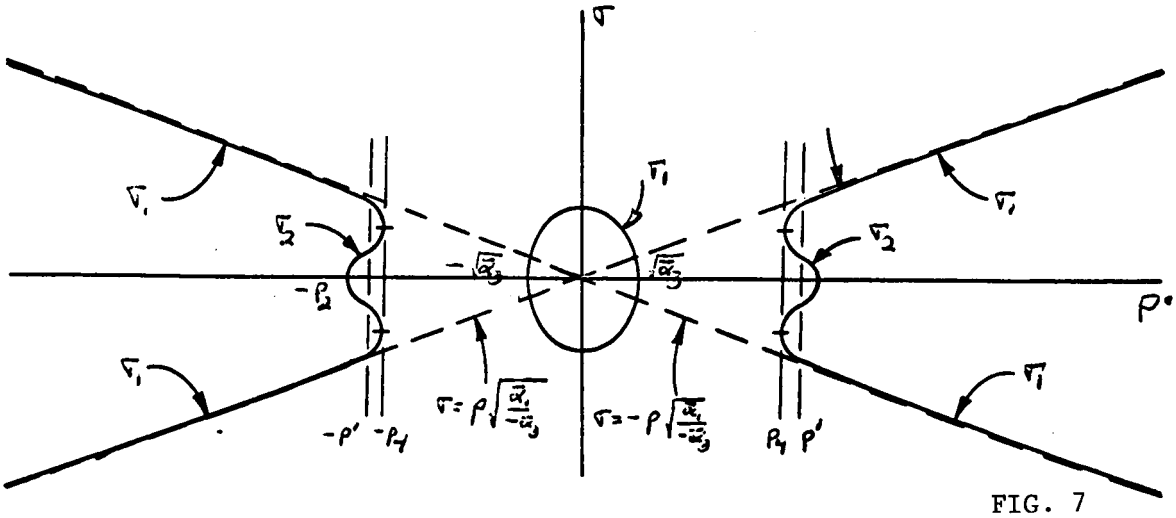

FIG. 7

Region D: $X^2 + Y^2 > 1 > \max [Y, X]$

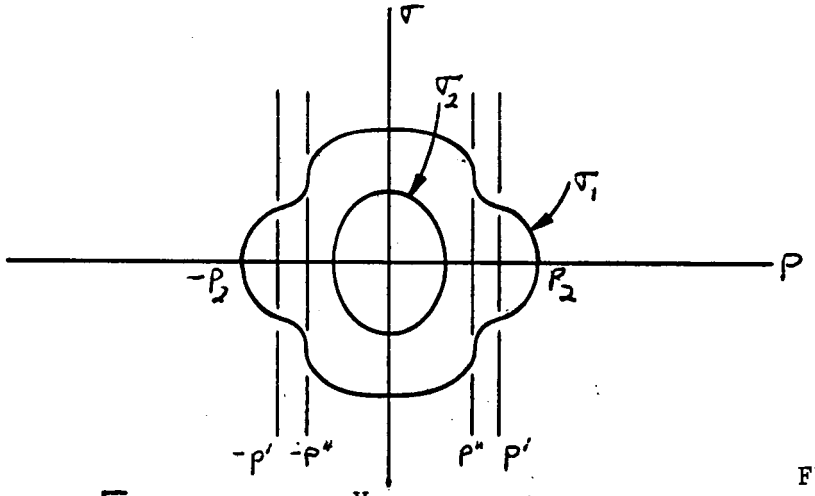

FIG. 8

Region E 1: $X < 1 < \min \left[Y, X + \frac{Y}{3Y - 2 + 2\sqrt{2Y(Y-1)}} \right]$

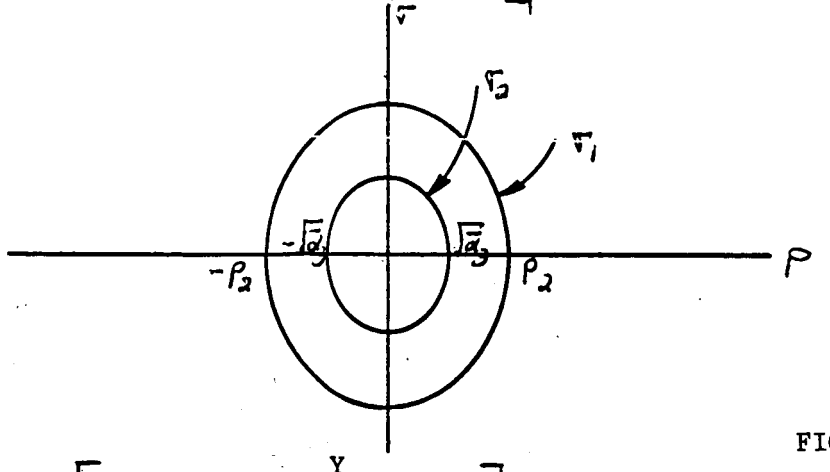

FIG. 9

Region E 2: $\max \left[X, X + \frac{Y}{3Y - 2 + 2\sqrt{2Y(Y-1)}} \right] < 1 < Y$

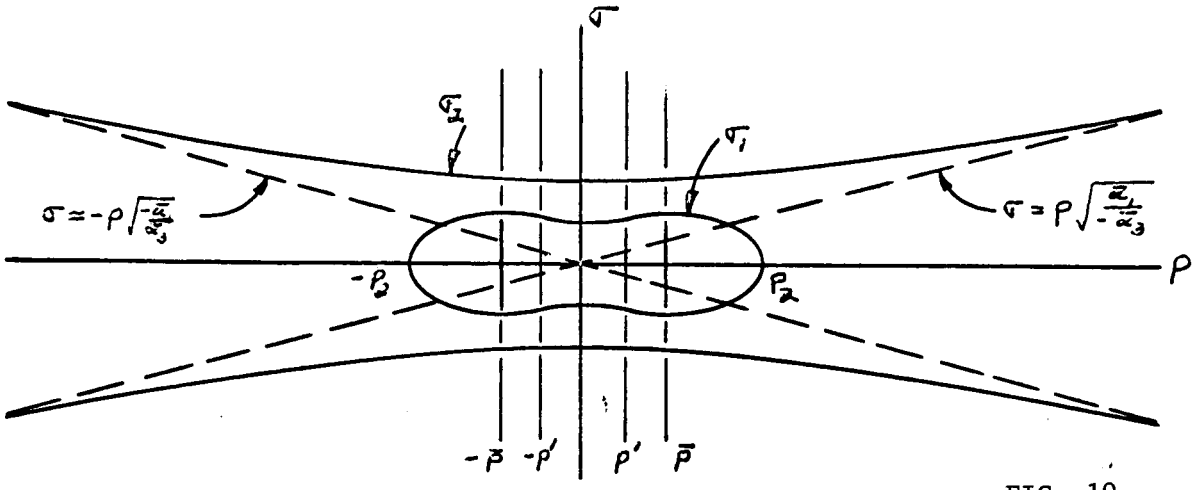

FIG. 10

Region F 1: $\min (Y, X) > 1 > \dfrac{2}{(2-X)(Y+2)}$

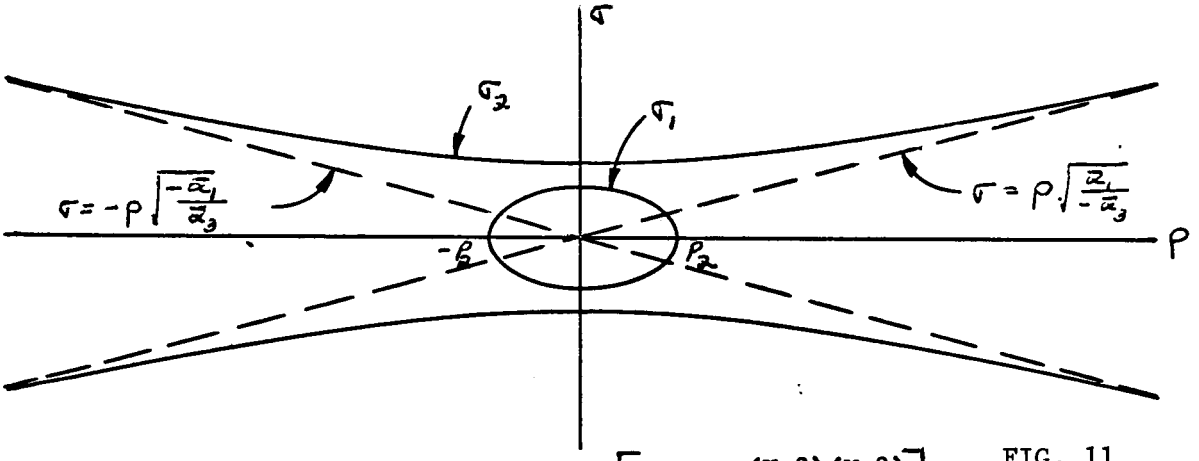

FIG. 11

Region F 2: $\min \left(X, \dfrac{2}{(2-X)(Y+2)}\right) > 1 > \max \left[X - Y, \dfrac{(X-2)(Y-2)}{2}\right]$

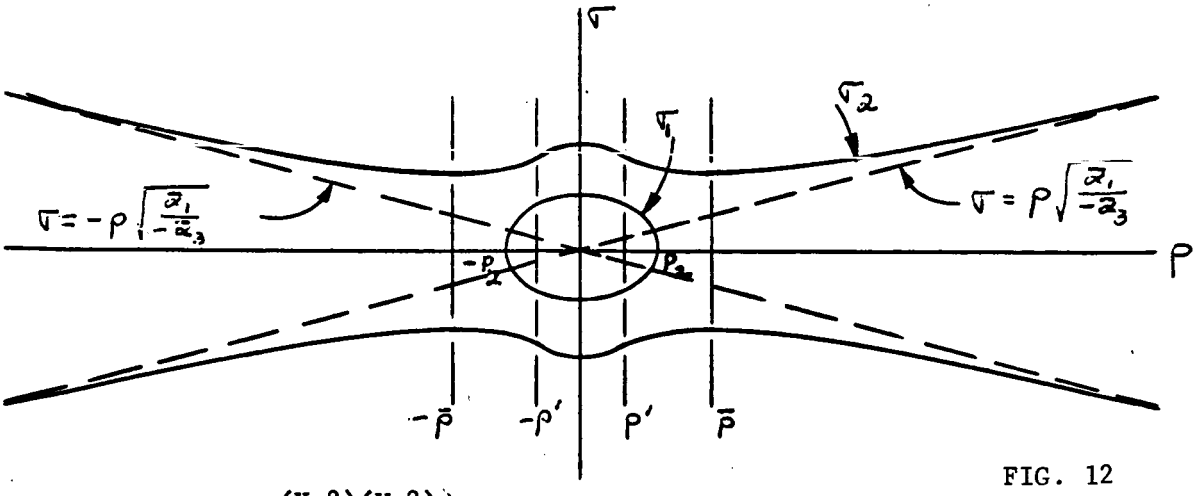

FIG. 12

Region F 3: $\min \left(X, \dfrac{(X-2)(Y-2)}{2}\right) > 1 > X - Y$

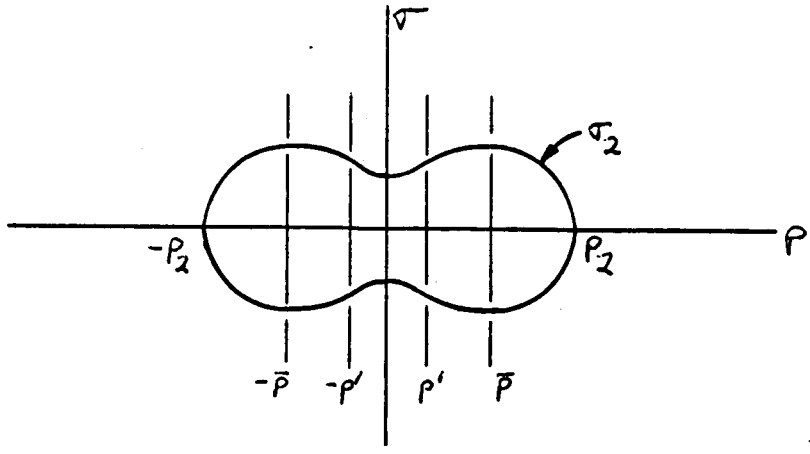

FIG. 13

Region G 1: $X > 1 > \max\left[Y, \frac{2}{(2-X)(Y+2)}\right]$

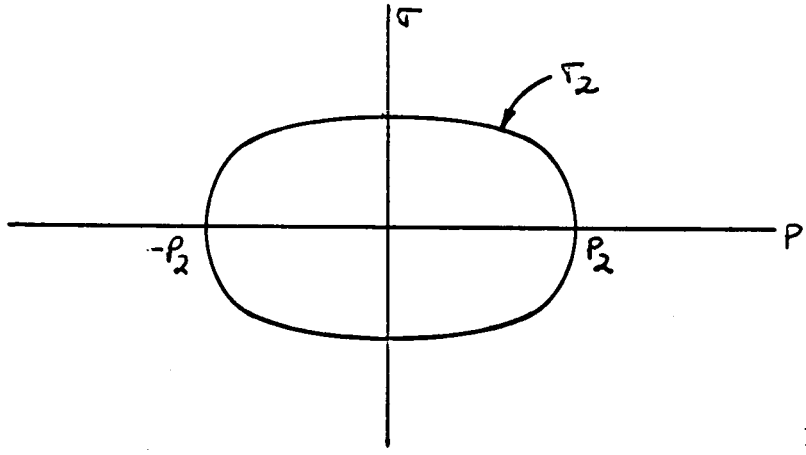

FIG. 14

Region G 2: $\left[\min\left[X, \frac{2}{(2-X)(Y+2)}\right] > 1 > \max\left[Y, X-YYY\right]\right.$

Region H: $X - Y > 1 > Y$

No curve.

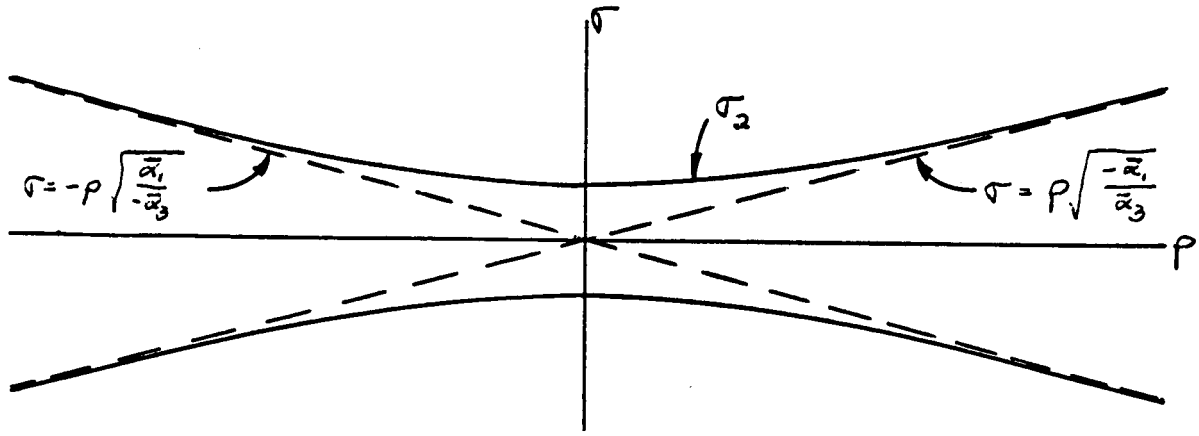

Region I 1: $\min [Y, X - Y] > 1 > \frac{(X-2)(Y-2)}{2}$

FIG. 15

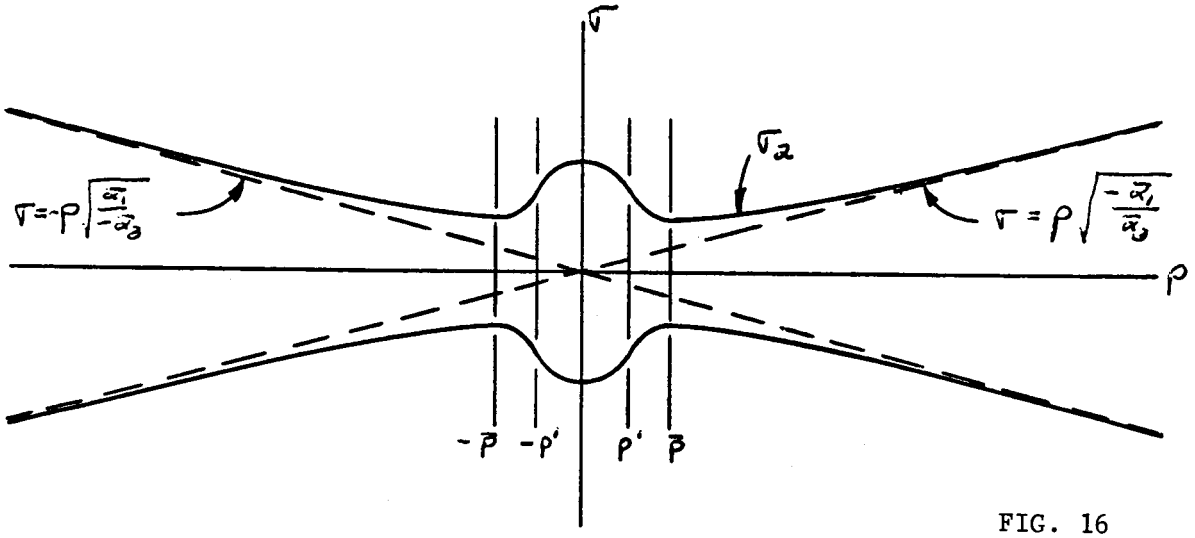

FIG. 16

Region I 2: $\min \left[Y, X - Y, \frac{(X-2)(Y-2)}{2}\right] > 1$

In addition to the previous curves it would be of interest to determine the curves at the boundaries between the regions. The curves for the boundaries between E 2 and E 1, between G 1 and G 2, between F 1 and F 2, between F 2 and F 3, and between I 1 and I 2 have already been discussed. We now look at the remaining boundaries.

At the boundary between Region A and Region B, when $X + Y = 1$, the curve for σ_2 shrinks to the single point at the origin while the curve for σ_1, remains the same as in both regions. At the boundary between Region B and Region C, when $X + Y^2 = 1$, the unbounded branch is not yet present (since when $X + Y^2 = 1$, $p_2 \to \infty$); thus we have only the curve for σ_1 as given in both regions. At the boundary between Region C and D, where $X^2 + Y^2 = 1$, σ_2 has a real value only at $p = \pm p_2$; thus, we have a dispersion curve for σ_1 as in Region C.

At the boundary between Region D and Region E, where $Y = 1$, $0 \leq X \leq 1$, the situation is somewhat more complex. σ_1 and σ_2 switch roles and the asymptotes coincide on the σ-axis. Thus for a graph of the dispersion curve we have (where we have not labeled σ_1 and σ_2)

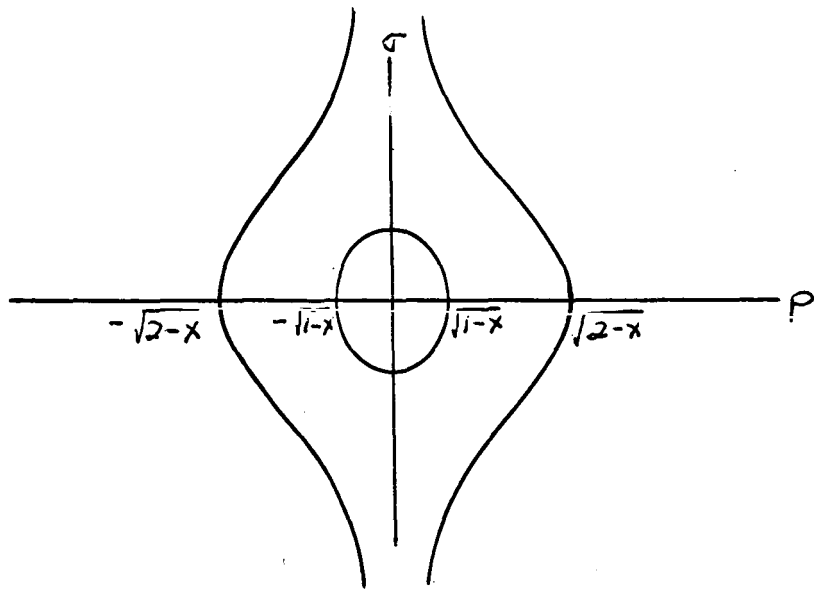

FIG. 17

At the boundary between Region G and Region F, where $Y = 1$, $1 \leq X \leq 2$, we have a bounded branch of the dispersion curve as given in the 2 regions. The unbounded branch does not appear until $Y > 1$. Again, as when $Y = 1$, $0 \leq X \leq 1$, the roles of σ_1 and σ_2 are interchanged.

Finally, at the boundary between Region F and Region I, where $X - Y = 1$, the curve for σ_1 reduces to the point at the origin and the curves for σ_2 remain the same as given in each of the regions.

2.2.2 Determination of the Far Field

The determination of the far field produced by a current distribution $\underset{\sim}{J}(\underset{\sim}{x}_1)$ follows from a straightforward application of (1). For a homogeneous isotropic medium, for which the Green's function $G(\underset{\sim}{x}-\underset{\sim}{x}_1)$ is known in closed form, this involves performing the indicated integrations to order 1/R, where $R = |\underset{\sim}{x} - \underset{\sim}{x}_1|$ is the mean distance from the current distribution to the (remote) field point. For a homogeneous anisotropic ionosphere, however, the Green's function is available only as a triple Fourier integral, so that the distance R is tied up with the angular variables. In addition, under some conditions focusing can take place so that the field no longer varies as 1/R.

The fact that R is large allows the evaluation of (1) to be performed by asymptotic methods. Thus, Arbel and Felsen [3] treated this problem in a rather general way for a collisionless ionosphere by applying the method of steepest descent. Their treatment included the investigation of special domains of the ionosphere parameters which can be encountered. However, the domains investigated by them do not include an important region of the VLF spectrum. Consequently, a brief derivation of the applicable relations will be given here for this case. The treatment will also be extended to include a small normalized collision frequency, since this is found to eliminate a singularity of the field due to a point source.

The treatment in this section is arranged as follows: Sec. 2.2.2.1 contains the preliminary reduction of the Green's function integrals to a form where an asymptotic evaluation may be performed. A first-order evaluation of the field is then carried out in Sec. 2.2.2.2 by the method of steepest descent, which is based on the stationary properties of the phase functions, for isolated stationary

points. The location of the stationary points requires a knowledge of the dependence of the phase function on the propagation constant parameter. This has been investigated in Sec. 2.2.1. The first-order technique of Sec. 2.2.2.1 is not applicable for propagation along the terrestrial magnetic field ($\theta = 0$), so this special case is treated in Sec. 2.2.2.4. The procedure of Sec. 2.2.2.1 also is based on the condition that the stationary points, if more than one exist, are well separated. In certain directions, two stationary points may coalesce to produce a focusing of rays, with corresponding enhancement of the field. In the neighborhood of such directions a revised procedure is necessary. This is sketched in Sec. 2.2.2.5.

2.2.2.1 Far Field of a Point Source

(1) for the field of a current distribution involves the Green's function expressed as a Fourier integral (12). The limits of the q-integrations in (12) run from $-\infty$ to ∞. This Green's function represents a spectrum of plane waves of all (including complex*) directions. N and D are, in general, fourth degree polynomials. Consequently, in integrating (1), the question of convergence arises. This is resolved by

---

* Complex directions correspond to waves having longitudinal components of field; i.e., TM- or TE-waves.

considering what is meant by a "point source."

A point source is the limit approached by a short current element as its length (measured in wavelengths) is reduced indefinitely. But in (12), the integration over q includes infinitesimally short wavelengths. Thus, although a point source is infinitesimally short compared to a wavelength in the medium, it is not infinitesimally short compared to the wavelength as $q \to \infty$ in the integral of (12). Hence, phase interference sets in between the field contributions due to the extremities of the point source as $q \to \infty$, and this insures convergence of the integral.

Writing the current distribution of the point source as

$$J(\underset{\sim}{x}_1) = \delta(\underset{\sim}{x}_1)\underset{\sim}{i}_c$$

where $\underset{\sim}{i}_c$ is a unit vector in the current direction and $\delta(\underset{\sim}{x}_1)$ is the Dirac δ-function, the x_1-integrations in (1) are readily performed [4], so that (1) becomes

$$\underset{\sim}{E}(\underset{\sim}{x}) = C \int d^3q \, \frac{N_{ji}(q)}{\Delta(q)} e^{-i\underset{\sim}{q}\cdot\underset{\sim}{\ell}} \underset{\sim}{i}_c \tag{24}$$

where

$$C = -\frac{i\omega\mu_0 k_0}{(2\pi)^3}, \tag{25}$$

The point of observation has the coordinates

$$(\rho \sin\theta\cos\phi, \rho\sin\theta\sin\phi, \rho\cos\theta)$$

where

$$\rho = k_0 R .$$

It is convenient to introduce cylindrical q-coordinates aligned with the terrestrial magnetic field direction. Thus, putting

$$q_1 = p\cos\beta$$
$$q_2 = p\sin\beta$$

and noting that there is no loss in generality in measuring β and φ from the

common x, x'-axis of the two coordinate systems (see Figs. 2 and 3 of [3]), (24) becomes

$$\underset{\sim}{E}(\underset{\sim}{x}) = C \int_0^\infty \rho d\rho \int_0^{2\pi} d\beta \int_{-\infty}^{\infty} dq_3 \frac{N_{ji}(q)}{\Delta(q)} \cdot \hat{\imath}_c \cdot e^{-i\rho[p\sin\theta\cos(\phi-\beta)+q_3\cos\theta} \tag{26}$$

The matrix N(q) will be written as N hereafter. D(q) is given by (13), which may be written as

$$\Delta = -\alpha_3(q_3^2-\sigma_1^2)(q_3^2-\sigma_2^2)$$

where the roots σ_1^2 and σ_2^2 are given by (15). (When collisions are present, $\bar{\alpha}_n$ is to be replaced by α_n.)

It should be noted that the roots do not depend on β. This corresponds to the property that the plane wave spectrum of the Green's function is symmetrical about the magnetic field direction.

The σ's depend on the ionosphere parameters through α_1 and α_3. It may be shown that, when collisions are present $\Im m(\sigma_{1,2}) < 0$. In the case being considered here, the normalized collision frequency is small. Consequently, $\sigma_{1,2}$ can be expanded in a power series in z to first order; i.e.

$$\sigma_{1,2}(p) = \bar{\sigma}_{1,2}(p) - iz\bar{\bar{\sigma}}_{1,2}(p) + O(z^2). \tag{27}$$

The expressions for $\bar{\sigma}$ and $\bar{\bar{\sigma}}$ are developed in Sec. 2.2.2.3. $\bar{\bar{\sigma}}$ is positive real, while, for the VLF case being considered here, $\bar{\sigma}_1$ is negative imaginary and $\bar{\sigma}_2$ is real. Hence, to $O(z^2)$, σ_1 is negative imaginary. This root corresponds to the ordinary wave, which is non-propagating at VLF. Thus, at VLF, the extraordinary wave is responsible for the propagated field.

The q_e-integration in (26) may now be performed by residues to yield

$$\underset{\sim}{E}(\underset{\sim}{x}) = i\pi C \int_0^\infty \rho d\rho \int_0^{2\pi} d\beta \frac{e^{-i\rho\rho\sin\theta\cos(\phi-\beta)}}{\alpha_3(\sigma_2^2-\sigma_1^2)} \left[\frac{N_1}{\sigma_1} e^{-i\rho|\cos\theta|\sigma_1} - \frac{N_2}{\sigma_2} e^{-i\rho|\cos\theta|\sigma_2}\right] \cdot \hat{\imath}_c \tag{28}$$

where $N_{1,2}$ denotes $N(\sigma_{1,2})$.

Since β does not enter into $\sigma_{1,2}$, the β-integration of (28) may be performed

to obtain Bessel functions of argument $w = \rho \sin\theta$. The integrals encountered are the following:

$$\left.\begin{aligned}
&\int_0^{2\pi} e^{-i w\cos\beta}\, d\beta = 2\pi J_0(w)\\
&\int_0^{2\pi} e^{-i w\cos\beta}\cos\beta\, d\beta = -i\,2\pi J_1(w)\\
&\int_0^{2\pi} e^{-i w\cos\beta}\sin^2\beta\, d\beta = 2\pi J_1(w)/w\\
&\int_0^{2\pi} e^{-i w\cos\beta}\sin\beta\cos\beta\, d\beta = 0 = \int_0^{2\pi} e^{-i w\cos\beta}\sin\beta\, d\beta
\end{aligned}\right\} w = \rho\sin\theta .$$

If these are combined with the proper components of N encountered in evaluating $\underset{\sim}{E}(\underset{\sim}{x})$, it is found that three types of integrals result:

$$\left.\begin{aligned}
&\int_0^{\infty} \{J_0(\rho w)\, L_0(\rho) \exp[-i\rho|\cos\theta|\sigma_{1,2}]\}\rho\, d\rho\\
&\int_0^{\infty} \{J_1(\rho w)\, L_1(\rho) \exp[-i\rho|\cos\theta|\sigma_{1,2}]\}\rho\, d\rho\\
&\int_0^{\infty} \{J_2(\rho w)\, L_2(\rho) \exp[-i\rho|\cos\theta|\sigma_{1,2}]\}\rho\, d\rho
\end{aligned}\right\} w = \rho\sin\theta \qquad (29)$$

where $L_0(\rho)$ and $L_2(\rho)$ are even functions of ρ, while $L_1(\rho)$ is an odd function of ρ. Since σ_1 and σ_2 are also even functions of ρ, as can be seen from (15). the $\{\ \}$-expressions in the integrands of all three of the integrals in (29) are even functions of ρ. Consequently the integration may be extended from to ∞ by use of the relation

$$2 J_n(\rho w) = H_n^{(2)}(\rho w) - e^{-i n\pi} H_n^{(2)}(-\rho w) .$$

Finally, except in the neighborhood of $\sin\theta = 0$ (this case will be treated in Sec. 2.2.2.4, the asymptotic form of the Hankel function may be used, since for the far field, the argument is large:

$$H_n^{(2)}(\rho w) \sim \left(\frac{2}{\pi\rho w}\right)^{\frac{1}{2}} e^{-i[\rho w - (n+\frac{1}{2})\frac{\pi}{2}]} , \qquad (30)$$

Correspondingly, the expression for the far field takes the form

$$\underset{\sim}{E}(\underset{\sim}{x}) = \frac{C_1}{(\rho \sin\theta)^{\frac{1}{2}}} \int_{-\infty}^{\infty} \frac{e^{-i p \rho \sin\theta}}{\sigma_1^2 - \sigma_2^2} \sum_{m=1}^{2} (-)^m \frac{\bar{N}(\sigma_m)}{\alpha_3 \sigma_m} e^{-i\rho|\cos\theta|\sigma_m} p^{\frac{1}{2}} dp \; \underset{\sim}{c} \tag{31}$$

where $\bar{N}(\sigma_n)$ is a matrix, and

$$C_1 = 2^{\frac{1}{2}} \pi^{\frac{3}{2}} e^{i\frac{3\pi}{4}} C \tag{31a}$$

2.2.2.2 First-Order Evaluation of Far Field

The expression for $\underset{\sim}{E}(\underset{\sim}{x})$ in (31) is now in the appropriate form for an asymptotic evaluation by the method of steepest descent [5]. (31) contains integrals of the form

$$I = \int_{-\infty}^{\infty} Q(p) e^{-i w M(p,\theta)} dp \tag{32}$$

where $w \gg 1$, and θ is a parameter independent of p, and

$$M(p,\theta) = p + |\tan\theta| \sigma_{1,2} .$$

The principal contribution to I comes from the range of p in the neighborhood of the stationary points p_j defined by

$$\frac{\partial}{\partial p} M(p,\theta)\Big|_{p=p_j} \equiv M^{(1)}(p_j) = 0. \tag{33}$$

Then $M(p, \theta)$ may be expanded in a power series around p_j, truncated at the first non-zero derivative of $M(p,\theta)$. If

$$M^{(2)}(p_j) \equiv \frac{\partial^2}{\partial p^2} M(p,\theta)\Big|_{p=p_j} \neq 0,$$

then

$$I \sim \sum_j \left(\frac{2\pi}{w|M^{(2)}(p_j,\theta)|}\right)^{\frac{1}{2}} Q(p_j) e^{-i w M(p_j,\theta) - i\pi/4 \operatorname{sgn}[M^{(2)}(p_j)]} . \tag{34}$$

Since $w = \rho \sin\theta$, the factor $w^{-\frac{1}{2}}$ in (34), together with the like factor $(\rho \sin\theta)^{-\frac{1}{2}}$ preceding the integral in (31) leads to the familiar $\rho^{-1} = 1/(k_o R)$ or inverse-distance dependence of E.

However, if, in the neighborhood of p_j, the condition

$$\frac{1}{2}(p-p_j)^2 M^{(2)}(p_j) >> \frac{1}{6}(p-p_j)^3 M^{(3)}(p_j) \tag{35}$$

is not satisfied, where $M^{(n)}(p_j) = [\partial^n M(p)/\partial p^n]|_{p = p_j}$, then (180) is not an accurate approximation. In particular, if

$$M^{(2)}(p_j) = 0 \tag{36}$$

then (34) is entirely inapplicable. This situation, which develops in the VLF case in the vicinity of certain angles $\theta = \theta_B$, will be treated in Sec. 2.2.2.5.

To apply the above method, it is first necessary to determine the stationary points. Since, in (27), z is small, we can regard $e^{-p|\cos\theta|z\bar{\sigma}_j}$ as part of the amplitude factor represented as Q(p) in (32). Furthermore, as noted earlier, $\bar{\sigma}_1$ is negative imaginary, corresponding to the fact that the ordinary wave does not propagate so that only σ_2 need be considered hereafter. Hence (33) yields for the stationary points

$$\frac{\partial}{\partial p}\left(p + |\tan\theta|\bar{\sigma}_2\right) = 0$$

or

$$\frac{\partial \bar{\sigma}_2}{\partial p} = -|\tan\theta| \ . \tag{37}$$

Since θ is the angle which the radius vector from the source to the observation point makes with the terrestrial magnetic field, (37) states that the stationary point occurs at the value of p where a line making the angle θ to the ordinate on a graph of $\bar{\sigma}_2$ vs. p is perpendicular to the curve. Thus it is now necessary to examine $\bar{\sigma}_2(p)$ to determine the values of θ for which (37) is satisfied. This is carried out in Sec. 2.2.2.3 for a typical VLF situation.

2.2.2.3 Variation of σ_2 With p

The expression for σ^2 in terms of the ionosphere parameters α_1 and α_3 is given by (15). These parameters are defined by

$$\alpha_1 = 1 - \frac{xu}{u^2 - y^2}$$

$$\alpha_3 = 1 - \frac{x}{u}$$

where

$$u = 1 - iz.$$

Writing

$$\alpha_1 = \bar{\alpha}_1 - iz\bar{\bar{\alpha}}_1 + O(z^2)$$

$$\alpha_3 = \bar{\alpha}_3 - iz\bar{\bar{\alpha}}_3 + O(z^2)$$

then we have

$$\bar{\alpha}_1 = 1 - \frac{x}{1-y^2}, \qquad \bar{\bar{\alpha}}_1 = x\frac{1+y^2}{(1-y^2)^2}$$

$$\bar{\alpha}_3 = 1 - x \qquad \bar{\bar{\alpha}}_3 = x \tag{38}$$

$$\frac{\bar{\alpha}_1}{\bar{\alpha}_3} = \frac{1-x-y^2}{(1-x)(1-y^2)}$$

At VLF, we have

$$x >> 1, \quad y^2 >> 1,$$

so that these become

$$\bar{\alpha}_1 \approx \frac{x}{y^2} \qquad \bar{\bar{\alpha}}_1 \approx \frac{x}{y^2} = \bar{\alpha}_1$$

$$\bar{\alpha}_3 \approx -x \qquad \bar{\bar{\alpha}}_3 \approx x \approx -\bar{\alpha}_3 \tag{38a}$$

$$\frac{\bar{\alpha}_1}{\bar{\bar{\alpha}}_3} \approx -\frac{1}{y^2}$$

In a typical VLF case, $\bar{\alpha}_1$ may be in the order of 10^0 to 10^2, while $\bar{\alpha}_3$ may be in the order of -10^2 to -10^6, so that $\bar{\alpha}_1/\bar{\alpha}_3$ is in the order of 10^{-3}.

$\sigma_{1,2}$ may be written in the form

$$\sigma_{1,2} = \left[\frac{U \mp (U^2+W)^{\frac{1}{2}}}{-2\alpha_3}\right]^{\frac{1}{2}} \tag{39}$$

where

$$U = p^2(\alpha_1 + \alpha_3) - 2\alpha_1\alpha_3$$

$$W = -4\alpha_3(p^2 - \alpha_3)(\alpha_1 p^2 - \alpha_1\alpha_3 - \alpha_1 + \alpha_3).$$

U and W, in turn, may be written in forms similar to (173):

$$U = U_1 - iz\,U_2 + O(z^2)$$

$$W = W_1 - iz\,W_2 + O(z^2) \tag{40}$$

where

$$U_1 = p^2(\bar{\alpha}_1 + \bar{\alpha}_3) - 2\bar{\alpha}_1\bar{\alpha}_3$$

$$W_1 = -4\bar{\alpha}_3(p^2 - \bar{\alpha}_3)(\bar{\alpha}_1 p^2 - \bar{\alpha}_1\bar{\alpha}_3 - \bar{\alpha}_1 + \bar{\alpha}_3) \qquad (40a)$$

$$U_2 = p^2(\bar{\bar{\alpha}}_1 + \bar{\bar{\alpha}}_3) - 2(\bar{\alpha}_1\bar{\bar{\alpha}}_3 + \bar{\bar{\alpha}}_1\bar{\alpha}_3$$

$$W_2 = \left(\frac{\bar{\bar{\alpha}}_3}{\bar{\alpha}_3} - \frac{\bar{\bar{\alpha}}_3}{p^2 - \bar{\alpha}_3} + \frac{\bar{\bar{\alpha}}_1 p^2 - \bar{\alpha}_1\bar{\bar{\alpha}}_3 - \bar{\bar{\alpha}}_1\bar{\alpha}_3 - \bar{\bar{\alpha}}_1 + \bar{\bar{\alpha}}_3}{\bar{\alpha}_1 p^2 - \bar{\alpha}_1\bar{\alpha}_3 - \bar{\alpha}_1 + \bar{\alpha}_3}\right) W_1 .$$

From (38a), $\bar{\alpha}_3$ is negative at VLF. Hence $\bar{\sigma}_1^2$ is negative, so that $\bar{\sigma}_1$ is imaginary, corresponding to a non-propagating wave. Thus we may confine attention to $\bar{\sigma}_2$ alone.

Introducing (40) into (15), and writing σ in the form (27), we obtain in

$$\bar{\sigma}_{1,2} = \left[\frac{U_1}{-2\bar{\alpha}_3} \mp \frac{(U_1^2 + W_1)^{\frac{1}{2}}}{-2\bar{\alpha}_3}\right]^{\frac{1}{2}} \qquad (41a)$$

$$\bar{\bar{\sigma}}_{1,2} = \frac{1}{2}\,\bar{\sigma}_{1,2}\left\{\frac{\left[U_2 \mp (U_1 U_2 + \frac{1}{2}W_2)(U_1^2 + W_1)^{-\frac{1}{2}}\right]}{-2\bar{\alpha}_3\,\bar{\sigma}_{1,2}^2} - \frac{\bar{\bar{\alpha}}_3}{\bar{\alpha}_3}\right\} \qquad (41b)$$

As already pointed out, σ_2 is an even function of p, so that a plot of $\bar{\sigma}_2$ or $\bar{\bar{\sigma}}_2$ vs. p will be symmetrical with respect to the ordinate p = 0.

For large p, $\bar{\sigma}_2$ approaches the asymptotic value

$$(\bar{\sigma}_2)_A = \pm(-\bar{\alpha}_1/\bar{\alpha}_3)^{\frac{1}{2}}\, p \qquad (42)$$

which represents straight lines through the origin of slope

$$(\partial\bar{\sigma}_2)_A/\partial p = \pm(-\bar{\alpha}_1/\bar{\alpha}_3)^{\frac{1}{2}} \approx \pm 1/y .$$

Furthermore it can be shown that, for the VLF conditions given by (38a), (41a) and (42) have no common root, so that the curve of $\bar{\sigma}_2$ vs. p never intersects the asymptotes.

To investigate the behavior of $\bar{\sigma}_2$ in the neighborhood of p = 0, (41b) may be expanded in a power series in p. This yields

$$\bar{\sigma}_2 = \left\{\bar{\alpha}_1\left[(\bar{\alpha}_1 - 1)(\bar{\alpha}_1 - \alpha_3)\right]^{\frac{1}{2}}\right\}^{\frac{1}{2}} - p^2\,\frac{\left\{\bar{\alpha}_1 + \bar{\alpha}_3 + \left[(\bar{\alpha}_1 - 1)(\bar{\alpha}_1 - \bar{\alpha}_3)\right]^{\frac{1}{2}}\right\}}{4\bar{\alpha}_3\left\{\bar{\alpha}_1 + \left[(\bar{\alpha}_1 - 1)(\bar{\alpha}_1 - \bar{\alpha}_3)\right]^{\frac{1}{2}}\right\}^{\frac{1}{2}}}$$

Since the coefficient of p is zero, $\partial\bar{\sigma}_2/\partial p = 0$ at $p = 0$. Furthermore, for the VLF case considered here, the second derivative there is negative, so that $\bar{\sigma}_2$ has a relative maximum at $p = 0$. In addition, $\partial\bar{\sigma}_2/\partial p = 0$ at $p = p_M$, where $\partial\bar{\sigma}_2/\partial p$ has a relative minimum, p_M being given by

$$p_M^2 = \frac{U_M + (U_M^2 + W_M)^{\frac{1}{2}}}{\bar{\alpha}_1(\bar{\alpha}_1 - \bar{\alpha}_3)^2}$$

$$\approx -\bar{\alpha}_3 = |\bar{\alpha}_3|$$

where

$$U_M = 2\bar{\alpha}_1\bar{\alpha}_3(\bar{\alpha}_1 - \bar{\alpha}_3)(\bar{\alpha}_1 - 1)$$

$$W_M = -\bar{\alpha}_1\bar{\alpha}_3(\bar{\alpha}_1 - \bar{\alpha}_3)^3(\bar{\alpha}_1 - 1)\left[(\bar{\alpha}_1 + \bar{\alpha}_3)^2 - (\alpha_1 - \alpha_3)(\alpha_1 - 1)\right].$$

Between the maximum of $\bar{\sigma}_2$ at $p = 0$ and the minimum at approximately $|\bar{\alpha}_3|^{\frac{1}{2}}$, there is an inflection point at an abscissa p_B. The expression for p_B is quite complicated, so that a numerical solution for it is required. However, a rough estimate of its location is that it is midway between the maximum and minimum. Thus we estimate that

$$p_B \approx p_M/2 \approx (-\bar{\alpha}_3)^{\frac{1}{2}}/2 .$$

It is then readily found that

$$\left|\tan\theta_B\right| = -\left.\frac{\partial\sigma_2}{\partial p}\right|_{p=p_B} \approx \frac{15}{4}\left(\frac{\bar{\alpha}_1}{-\bar{\alpha}_3}\right)^{\frac{1}{2}} = \frac{15}{4}\left|\tan\theta_A\right|.$$

Thus, for the type of VLF situation considered here, where

$$-\bar{\alpha}_3 >> \bar{\alpha}_1 >> 1,$$

the slope of the $\bar{\sigma}_2$-curve is steepest at the inflection point, where it is approximately four times the slope of the asymptotes.

From the above developments, a graph of $\bar{\sigma}_2$ vs p has the general form shown in Fig. 18. The slope of this curve is $\partial\bar{\sigma}_2/\partial p$. This slope is zero at $p = 0$, decreases with increasing p to a minimum (i.e., maximum negative) value

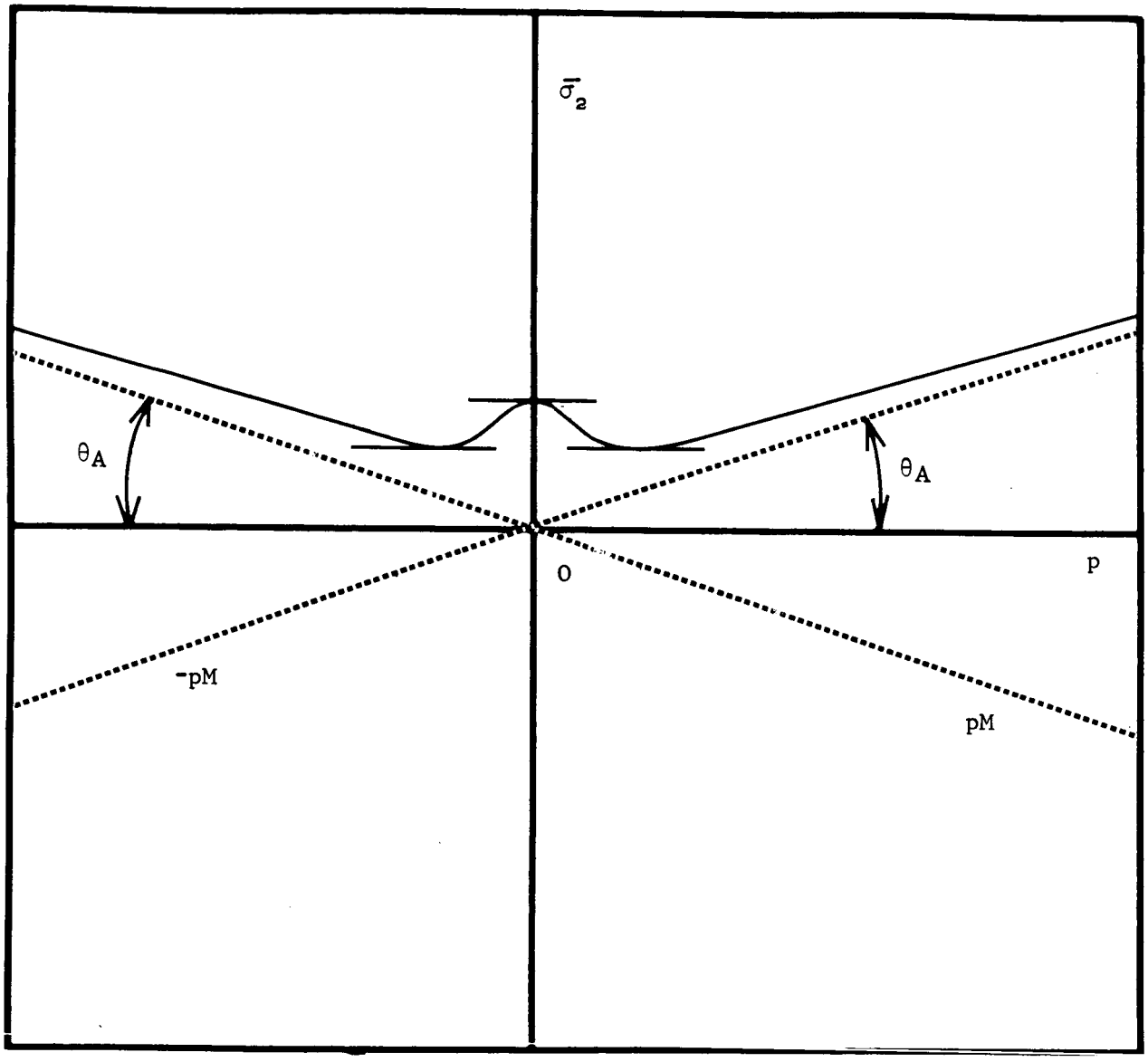

Fig. 18 Plot of $\bar{\sigma}_2(p)$

at an inflection point p_B, then increases again to zero at $p = p_M$, and from there on is positive. As $p \to \infty$, the slope approaches asymptotically the value $\tan \theta_A$, where

$$\tan \theta_A = (-\alpha_1/\alpha_3)^{\frac{1}{2}} = 1/y ,$$

where y is the normalized gyro frequency. For negative p, the curve is the mirror image of the positive branch.

Typical values of θ_A are in the order of a few degrees.

Similarly, a graph of $\bar{\bar{\sigma}}_2$ vs. p is shown in Fig. 19. This has a monotonic increase from a minimum at p = 0 to the same asymptotic value as $\bar{\sigma}_2$.

From Fig. 18, the following conclusions are obvious:

(a) For $\theta < \theta_B$, where

$$\tan \theta_B = -\left|\left(\partial \bar{\sigma}_2/\partial p\right)_{p=p_0}\right|$$

there are two stationary points if $\tan \theta > \tan \theta_A$ (from the positive branch in the region $0 < p < p_M$), or three, if $\tan \theta < \tan \theta_A$ (the additional one from the negative branch in the region $-\infty < p < -p_M$).

(b) For $\theta = \theta_B$;

$$\partial^2 \bar{\sigma}_2/\partial p^2 = 0 ;$$

consequently (34) is no longer applicable for angles in the vicinity of θ_B, since the condition (35) is violated. It is then necessary to perform a second-order evaluation of the integral (32). This is investigated in Sec. 2.2.2.5.

(c) For $p > p_M$, there is no stationary point for $\theta > \theta_A$. Thus, short-wavelength components of the plane-wave spectrum cannot propagate at an angle greater than θ_A to the magnetic field.

For $\theta \to \theta_A$, which is case (a) above, there are three stationary points. The contribution of the stationary point from the part of the curve approaching

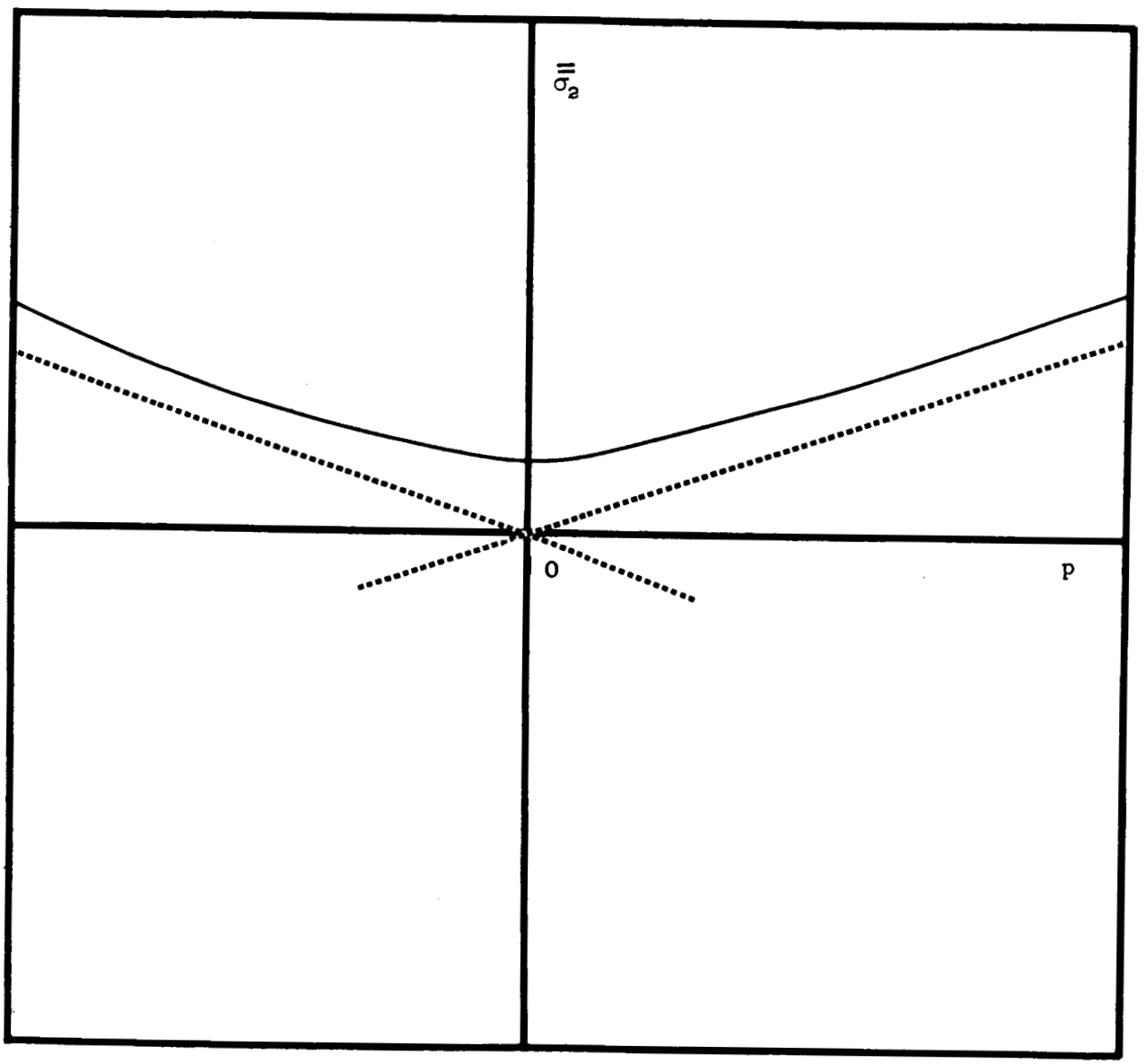

Fig. 19 Plot of $\bar{\bar{\sigma}}_2$ (p)

the asymptote, is easily shown to be negligible because of the effect of collisions. This is due to the factor

$$e^{-\rho|\cos\theta|z\,\bar{\bar{\sigma}}_2}$$

which is taken into the amplitude factor Q(p) in (32). As shown in (41b), $\bar{\bar{\sigma}}_2 \propto \bar{\sigma}_2$, while from (42), $\bar{\sigma}_2 \to \infty$, $sp \to \infty$, corresponding to θ_A. Thus the above exponential factor reduces the contribution of this stationary point to a vanishing small value.

In the work of Arbel and Felsen [3], where collisions are neglected, a singularity of the far field develops for $\theta = \theta_A$ due to the contribution from the asymptotic part of the σ_2 vs. p curve. In order to overcome this, it was necessary for them to revert to a distributed source in order to obtain a convergent spectrum. The inclusion of collisions, however, avoids this because of the exponential attenuation factor.

For an isolated stationary point p_1, where (34) is applicable, the expression (31) for the field becomes

$$\underset{\sim}{E}(\underset{\sim}{x}) = \frac{C_1}{\rho\sin\theta}\left(\frac{2\pi}{|M^{(2)}|}\right)^{\frac{1}{2}} e^{-\rho z|\cos\theta|\bar{\bar{\sigma}}_2(p_1)}\, e^{-i\rho\sin\theta M_1 - i\frac{\pi}{4}\operatorname{sgn}(M^{(2)})}\,\bar{\bar{L}}(p_1)\cdot\underset{\sim}{i}_c \tag{43}$$

where

$$M_1 = p_1 + |\tan\theta|\,\bar{\sigma}_2(p_1)$$

$$M^{(2)} = |\tan\theta|\frac{\partial^2}{\partial p^2}\,\bar{\sigma}_2(p)\Big|_{p=p_1}$$

and $\bar{\bar{L}}(p_1)$ is the matrix

$$\bar{\bar{L}}(p_1) = \frac{-p^{\frac{1}{2}}}{\bar{\alpha}_3\,\bar{\sigma}_2\left(\bar{\sigma}_2^2 - \bar{\sigma}_1^2\right)}\Big|_{p=p_1} \cdot \bar{\bar{N}}\left(\bar{\sigma}_2(p_1)\right).$$

From (43), since $\bar{\bar{L}}(p_1)$ is a matrix, it is evident that the field is elliptically polarized, in general. Furthermore, (43) gives the contribution of a single stationary point. If more than one stationary point exists, each will yield a contribution of the form (43). The vector sum of the several

contributions then will depend on distance, since, in general, M_1 will not be the same for the several stationary points, so that an interference pattern will develop.

The type of result (43) ceases to hold where two stationary points approach each other, i.e., in the neighborhood of inflection points p_B, and where the asymptotic expansion of the Hankel function, (30), breaks down, i.e., in the neighborhood of $\sin\theta = 0$. In the former case, a second-order evaluation of the integral (32) is necessary; this is outlined in Sec. 2.2.2.5. In the latter case, a revised procedure, which is developed in Sec. 2.2.2.4, is necessary.

2.2.2.4 The Case $\sin\theta \approx 0$

When the observation point is in, or nearly in, the direction of the magnetic field, the asymptotic expansion (30) no longer is usable, for then the argument

$$pw = p\rho \sin\theta$$

is not sufficiently large to satisfy the condition $pw \gg 1$. This condition is violated in the vicinity of $\theta = 0$. According to the first-order evaluation in Sec. 2.2.2.2, the maximum and minimum locations $p = 0$ and $p = p_M$ are stationary points for $\theta = 0$. Consequently the first-order evaluation of Sec. 2.2.2.2 is inapplicable in that case.

The applicability of the asymptotic expansion is determined by the magnitude of the argument, which in the present case is composed of the three factors ρ, $\sin\theta$, and p. Thus, for an arbitrarily small, yet finite, value of $\sin\theta$, the argument can be made sufficiently large by making the product ρp large enough. For the stationary point p_M, which is large, this is feasible, but not for $p = 0$. Thus it suffices to consider the limiting case $\sin\theta = 0$, since the procedure then will apply both to p_M for $\sin\theta \equiv 0$, and to $p = 0$.

For $\theta = 0$, $pw = p\rho \sin\theta = 0$, so that $J_n(pw) = 0$ except for $n = 0$, for which $J_0(pw) = 1$. Consequently only the first type of integral in (29) survives. Furthermore, $L_0(p)$ contains terms with p^{2m}, where $m = 0, 1, 2$. The pertinent integral thus is

$$I = \int_C^{\infty} p^{2m+1} e^{-i\rho\sigma_2} dp = e^{-\rho z \bar{\bar{\sigma}}_2} \int_0^{\infty} p^{2m+1} e^{-i\rho\bar{\sigma}_2} dp$$

This has stationary points at $\partial\bar{\bar{\sigma}}_2/\partial p = 0$. A first-order evaluation of the integral around a stationary point P_S thus is

$$I_S = e^{-\rho z \bar{\bar{\sigma}}_2(p_S)} e^{-i\rho\bar{\sigma}_2(p_S)} \int_0^{\infty} p^{2m+1} e^{-i\frac{1}{2}\rho(p-p_S)^2\bar{\sigma}_2^{(2)}(p_S)} dp$$

For $P_S = 0$, the magnitude of the integral in this expression is

$$\frac{m!}{2\left[\frac{1}{2}\rho\sigma_2^{(2)}(0)\right]^{m+1}}$$

Thus the decrease of the field with distance is at least as rapid as ρ^{-1}.

On the other hand, for $P_S = P_M$, which in the VLF case is

$$p_M = (-\alpha_3)^{\frac{1}{2}}$$

and thus very large, the factor p^{2m+1} in the integral is slowly varying in the neighborhood of the stationary point, so that it may be set equal to p_M^{2m+1} and taken out from under the integral. The result then becomes

$$I \sim \left(\frac{\pi}{2\rho\bar{\sigma}_2^{(2)}(p_M)}\right)^{\frac{1}{2}} p_M^{2m+1} e^{-\rho z \bar{\bar{\sigma}}_2(p_M)} e^{-i\rho\bar{\sigma}_2(p_M) - i\frac{\pi}{4}} \tag{44}$$

An equal contribution results from the stationary point at $-P_M$, so that the above value is doubled. This leads to a distance dependence of the field of $\rho^{-\frac{1}{2}}$.

The angle over which the result (44) holds is a function of distance, since, as already pointed out, for any finite value of $\sin\theta$ the product pw becomes large at a sufficiently large distance. The $\rho^{-\frac{1}{2}}$ dependence for $\theta = 0$ corresponds to the fact that in this direction propagation is two-dimensional.

Of the three stationary points at $\theta = 0$, the one at $p = 0$ is of lower order in the far field than those at $p = |p_M|$.

2.2.2.5 Second-Order Evaluation of Far Field

In the first-order evaluation of (32), $M(p,\theta)$ is expanded in a power series, which is terminated at the second degree term, on the assumption that higher order terms are negligible in comparison to it. Specifically, this demands that (35) be satisfied. In the neighborhood of p_B, where (36) holds, this condition is violated, so that it is necessary to carry the power series expansion to include the third degree term, which involves $M^{(3)}(p)$.

The vanishing of the second derivative is due to the coalescence of two neighboring stationary points p_1, p_2. Both of these satisfy (33), which leads to (37). It is then preferable to expand the exponential about the point p_B rather than the stationary point(s). This is accomplished by writing the exponent as

$$-i\,M(p,\theta) = -i\left[M_B + (p-p_B)M^{(1)} + \frac{1}{3!}(p-p_B)^3 M^{(3)}\right]$$

$$= -i\,M_B + \gamma^2 t - t^3/3$$

where

$$t = \left[i\,\tfrac{1}{2}M^{(3)}\right]^{\frac{1}{3}}(p-p_B)$$

$$\gamma^2 = -i\,M^{(1)}$$

and

$$M_B = M(p_B,\theta)$$

$$M^{(n)} = \frac{\partial^n M(p,\theta)}{\partial p^n}\bigg|_{p=p_B}.$$

The exponent has stationary points at $t_{1,2} = \pm\gamma$, and these must be made to coincide with p_1, p_2. Hence

$$\gamma^3 = -i\,\tfrac{3}{4}\left[M(p_1,\theta) - M(p_2,\theta)\right].$$

With the exponent in the above form, the integration path passes through the three points $t = \gamma$, 0, $-\gamma$ and passes off to infinity along steepest descent

lines from $\pm\gamma$ [6]. The integral then leads to the Airy functions, or, alternatively, the modified Hankel functions of order one-third [7]. The result is that the field becomes

$$\underset{\sim}{E}(\underset{\sim}{x}) = \frac{2\pi C_1}{(\rho\sin\theta)^{\frac{5}{6}}}\left(\frac{2}{M^{(3)}}\right)^{\frac{1}{3}} e^{-\rho z|\cos\theta|}\bar{\bar{\sigma}}_2(p_B)\, e^{-i\rho\sin\theta M_B}\, A i(r^2)\,\bar{L}(p_B)\cdot\underset{\sim}{i}_c \qquad (45)$$

A notable feature of this result is that the field varies with distance as $\rho^{-5/6}$, which is slower than the normal ρ^{-1}. This is due to focusing which results from the coalescence of the two stationary points at $\theta = \theta_B$. As in the case of $\theta = 0$, the angular range of (45) decreases with increasing distance.

Since θ_B is the maximum angle at which a stationary point occurs, the angle θ_B represents the boundary of the cone of propagating rays. For $\theta > \theta_B$, no propagation takes place. In Sec. 2.2.2.3 an estimate of θ_B was given as approximately four-times θ_A. Thus, typical values of θ_B at VLF are around 10°.

2.3 IMPEDANCE OF AN ELECTRICALLY SMALL LOOP

In SR 1 the analysis of the impedance of an electrically small loop was given. This was left in a form which required numerical integrations to evaluate the radiation resistance. Further work has led to a simple closed form result for the limiting cases of loop axis parallel and perpendicular to the terrestrial magnetic field. From these results it is found that the radiation resistance of an electrically small loop is many orders of magnitude higher in the ionosphere than in free space and varies only a small amount with orientation. The loop thus appears to be an almost ideal type of radiator for VLF frequencies in the ionosphere.

2.3.1 Discussion of Loop Impedance Properties

The impedance of an electrically small loop was reduced to the form

$$Z = Z_1 + Z_{21} + Z_{22}$$

where

$$Z_1 = i\,120\pi A \log\left(\frac{4}{\epsilon} - \frac{1}{2}\right) = i\,120\pi A \log\left(\frac{4A}{a} - \frac{1}{2}\right) \tag{46}$$

$$Z_{21} = \frac{-15A^2}{2\pi} \int_0^{\pi} \sin\mu\, d\mu \sum_{n=1}^{\infty} \frac{(-1)^n (2A)^{2n} M_{2n}}{(2n)!} \left\{ \frac{-Q_{2n} C_{n+1}}{r_1 + r_2} + \frac{C_n}{r_1 + r_2} \left[\frac{-(\alpha_1\alpha_3 - \alpha_1^2 + \alpha_2^2)\sin^2\theta \sin^2\mu\, Q'_{2n-2} + \alpha_1\alpha_3 Q_{2n}}{\alpha_1 \sin^2\mu + \alpha_3 \cos^2\mu} \right] \right\} \tag{47}$$

$$Z_{22} = \frac{-15iA^2}{2\pi} \int_0^{\pi} \sin\mu\, d\mu \sum_{n=1}^{\infty} \frac{(-1)^n (2A)^{2n-1} M_{2n-1}}{(2n-1)!} \left\{ -Q_{2n-1} d_n + d_{n-1} \left[\frac{-(\alpha_1\alpha_3 - \alpha_1^2 + \alpha_2^2)\sin^2\theta \sin^2\mu\, Q'_{2n-3} + \alpha_1\alpha_3 Q_{2n-1}}{\alpha_1 \sin^2\mu + \alpha_3 \cos^2\mu} \right] \right\} \tag{48}$$

A is the electrical circumference of the loop, and a the electrical half-width of the strip cross section considered.

Since the inductance of the strip loop is

$$L = \mu_0 \frac{A}{k_0} \left(\log \frac{4A}{a} - \frac{1}{2} \right),$$

its reactance is

$$i\omega L = i\mu_0 \pi f A \log\left(\frac{4A}{a} - \frac{1}{2}\right)$$

$$= i\,120\pi A \log\left(\frac{4A}{a} - \frac{1}{2}\right) = Z_1 .$$

Consequently, Z_1 is precisely the inductive reactance of the loop, and it is independent of the ionosphere parameters or loop orientation.

(47) and (48) are complicated expressions for Z_{21} and Z_{22}. However, it is possible to simplify these greatly by virtue of the fact that the loop is electrically small, so that A is a small quantity. Hence, in the summations in (47) and (48) we need retain only the first term. This gives

$$Z_{21} = 30\pi A^4 \int_0^{\pi} \sin\mu \, d\mu \left\{ \frac{Q_2 c_2}{r_1 + r_2} + \frac{c_1}{r_1 + r_2} \left[\frac{(\alpha_1\alpha_3 - \alpha_1^2 + \alpha_2^2) \sin^2\theta \sin^2\mu \, Q_0' - \alpha_1\alpha_3 Q_2}{\alpha_1 \sin^2\mu + \alpha_3 \cos^2\mu} \right] \right\} \tag{49a}$$

$$Z_{22} = i\frac{80}{\pi} A^3 \int_0^{\pi} \sin\mu \, d\mu \left\{ Q_1 d_1 + d_0 \left[\frac{(\alpha_1\alpha_3 - \alpha_1^2 + \alpha_2^2) \sin^2\theta \sin^2\mu \, Q_{-1}' - \alpha_1\alpha_3 Q_1}{\alpha_1 \sin^2\mu + \alpha_3 \cos^2\mu} \right] \right\} . \tag{49b}$$

In the free-space case, Z_{21} reduces to

$$Z_{21} = R_{FS} = 80\pi^2 A^4 \tag{50}$$

which is the familiar radiation resistance of a small loop [8]. Z_{22}, in the free-space case, is purely imaginary. Since it is of order A^3, it is negligible relative to the reactance Z_1, which is of order A.

In general, both Z_{21} and Z_{22} have real and imaginary parts. This is partly due to the effect of collisions. Even in the collisionless case, however, the integrals in Z_{21} and Z_{22} have both real and imaginary components when α_1 and α_3 have opposite signs. This situation prevails in the VLF case being considered here. The imaginary (reactive) parts of Z_{21} and Z_{22} should be negligible relative to Z_1, since they are of order A^4 and A^3, respectively, while Z_1 is of order A. The real part of Z_{21} is of order A^4, and this is the order of the free-space resistance (50). The real part of Z_{22}, on the other hand, represents a resistance of order A^3. Consequently, a loop radiates more efficiently at VLF in the ionosphere than in free space.

In view of the importance of this conclusion, it is of interest to determine the properties of this resistance term which arises from Z_{22}. Since the Q-terms involve a β-integration, a double integration is involved. One of these integrations may be performed by transforming from (μ,β)-coordinates back to (σ,ϕ)-coordinates and carrying out the σ-integration. This gives

$$Z_{22} = \frac{-i\,160A^3}{\sqrt{\alpha_1\alpha_3}} \left\{ \int_0^{\pi/2} \left[X_{22}^{(1)} + X_{22}^{(2)} + X_{22}^{(3)} \right] \frac{d\phi}{R} \right\} - i\,80\pi A^3 (1 - 4\cos^2\theta) \tag{51}$$

where $R = \left[1 - \left(1 - \frac{\alpha_1}{\alpha_3} \right) \sin^2\theta \sin^2\phi \right]^{\frac{1}{2}}$. The last term in the braces is a pure reactance, so that it does not represent a radiation resistance term, and so may

be neglected in the present discussion. The factors $X_{22}^{(1),(2),(3)}$ are

$$X_{22}^{(1)} = 2(\alpha_3 - \alpha_1)\left[\cos^2\theta(1+2\sin^2\theta) + \frac{\alpha_1}{\alpha_3-\alpha_1}(\cos^2\theta - \sin^2\theta)\right],$$

$$X_{22}^{(2)} = \left[-\alpha_1(\alpha_3-1) - 2(\alpha_3-\alpha_1)\sin^2\theta\cos^2\theta(1+\cos^2\phi)\right]\left[1 - \frac{\alpha_1-\alpha_3}{\alpha_3}\,\frac{\cos^2\theta - \sin^2\theta\cos^2\phi}{\left(\sqrt{\frac{R}{\alpha_1}} + \sqrt{\frac{\alpha_1}{\alpha_3}}\right)^2}\right],$$

$$X_{22}^{(3)} = -4(\alpha_3-\alpha_1)(\cos^2\theta - \sin^2\theta)\sin^2\theta\cos^2\theta\cos^2\phi\,\frac{(\alpha_1-\alpha_3)/\alpha_3}{\left(R + \sqrt{\frac{\alpha_1}{\alpha_3}}\right)^2}.$$

The factor $(\alpha_3)^{-\frac{1}{2}} = -i(x-1)^{\pm\frac{1}{2}}$, where x is the square of the normalized plasma frequency, is negative imaginary in the collisionless VLF-case ($x \gg 1$). Hence, in the range of ϕ for which the radicand in the denominator of (51) is positive, a resistance term results. This range of ϕ is 0 to $\sin^{-1}\{(1-\alpha_1/\alpha_3)^{\frac{1}{2}}\sin\theta\}$ or $\pi/2$, whichever is smaller.

Fortunately, it is possible to carry out the final ϕ-integration of (51) for $\theta = \pi/2$ in the nearby collisionless case. (It is still necessary to retain a small collision term in the radicand to keep Z_{22} finite) Since the integral becomes trivial for $\theta = 0$, we can also obtain the range of variation of the resistive component of Z_{22} with the loop orientation θ.

For $\theta = \pi/2$,

$$X_{22}^{(1)} = -2\alpha_1$$

$$X_{22}^{(2)} = -\alpha_1(\alpha_3-1)\left[1 - \frac{k^2\cos^2\phi}{(R+b)^2}\right] \approx -\alpha_1\alpha_3\left[1 - \frac{k^2\cos^2\phi}{(R+b)^2}\right]$$

$$X_{22}^{(3)} = 0$$

where

$$b = \sqrt{\frac{\alpha_1}{\alpha_3}}, \qquad (52)$$

$$k^2 = \frac{\alpha_3 - \alpha_1}{\alpha_3} = 1 - b^2 \quad , \tag{53}$$

$$R = \sqrt{1 - k^2 \sin^2 \phi} \quad , \tag{54}$$

In the VLF case of interest here, where the normalized ionosphere parameters x and y are large, and z is small,

$$\alpha_1 \approx \frac{x}{y^2}(1 - iz) \quad ,$$

$$\alpha_3 \approx -x(1 + iz) \quad ,$$

and

$$\alpha_1 \alpha_3 \approx -\frac{x^2}{y^2} + i\frac{x^2 z}{y^4} \quad ,$$

so that $X_{22}^{(1)}$ is negligible in comparison with $X_{22}^{(2)}$. Also

$$\frac{\alpha_1}{\alpha_3} = b^2 \approx -\frac{1}{y^2}(1 - i2z) \, .$$

Consequently

$$\sqrt{\alpha_1 \alpha_3} \approx -i\frac{x}{y} \quad ,$$

$$b \approx -i\frac{1}{y} \, . \tag{52a}$$

Then

$$k^2 = 1 - b^2 = 1 + \frac{i}{y^2} - i\frac{2z}{y^2} \, . \tag{53a}$$

Thus the real part of R^2 vanishes in the range of integration at an angle ϕ_1 given by

$$\sin \phi_1 = \left(1 + \frac{1}{y^2}\right)^{-\frac{1}{2}} \quad ,$$

or

$$\tan\phi_1 = \gamma. \tag{55}$$

Thus

$$R(\phi_1) = \left(-\lambda\frac{2z}{y^2}\right)^{\frac{1}{2}}. \tag{54a}$$

For $\phi > \phi_1$, the real part of R^2 becomes negative, so that R becomes approximately purely imaginary. Thus this range of ϕ contributes a reactance term, with which we are not concerned. Hence, to find the resistance contribution, R_{22}, of (105) we replace the upper limit of the integral by ϕ_1. Then

$$\begin{aligned} R_{22}\Big|_{\theta=\pi/2} &= \lambda 160A^3\sqrt{\alpha_1\alpha_3}\,\mathrm{Re}\left\{\int_0^{\phi_1}\frac{1}{R}\left[1-\frac{k^2\cos^2\phi}{(R+b)^2}\right]d\phi\right\} \\ &= 160A^3\left(\frac{x}{y}\right)\cdot\mathrm{Re}\{I\}. \end{aligned} \tag{56}$$

In the integrand, we write

$$\frac{1}{(R+b)^2} = \frac{(R-b)^2}{(R^2-b^2)^2} = \frac{R^2+b^2-2bR}{(R^2-b^2)^2}.$$

But, since $k^2 = 1-b^2$,

$$R^2-b^2 = 1-(1-b^2)\sin^2\phi-b^2 = (1-b^2)\cos^2\phi,$$

$$R^2+b^2 = (1-b^2)\cos^2\phi+2b^2.$$

Hence

$$1-\frac{k^2\cos\phi}{(b+R)^2} = -\frac{2b^2+2bR}{(1-b^2)\cos^2\phi},$$

so that

$$\int_0^{\phi_1}\frac{d\phi}{R}\left[1-\frac{k^2\cos^2\phi}{(b+R)^2}\right] = -\frac{2b^2}{1-b^2}\int_0^{\phi_1}\frac{d\phi}{R\cos^2\phi}-\frac{2b}{1-b^2}\int_0^{\phi_1}\frac{d\phi}{\cos^2\phi}$$

$$= -\frac{2b^2}{1-b^2}\left\{F(\phi_1)+\frac{1}{b^2}\left[R(\phi_1)\tan\phi_1-E(\phi_1)\right]\right\}-\frac{2b}{1-b^2}\tan\phi_1,$$

where $F(\phi_1,k)$ and $E(\phi_1,k)$ are the elliptic integrals of the first and second kind, respectively. Since, from (52a), b is almost purely imaginary, the last term does not contribute a resistance term. Further, from (54a) and (55),

$$R(\phi_1)\tan\phi_1 = (2z)^{\frac{1}{2}} e^{-z}\frac{\pi}{4}$$

which is very small in virtue of the condition $z \ll 1$. Hence we obtain

$$\mathrm{Re}\{I\} \simeq \frac{2}{y^2}\left[F(\phi_1,k) + y^2 E(\phi_1,k)\right].$$

Since, from (55), $\phi_1 = \tan^{-1} y \approx \pi/2$, and from (53a) $k^2 = 1-b^2 \approx 1 + 1/y^2 \approx 1$, we have

$$E(\phi_1,k) \approx 1$$

$$F(\phi_1,k) = \frac{2\phi_1}{\pi} F\left(\frac{\pi}{2},k\right) - O\left(\frac{1}{y}\right) \approx \log(4y).$$

Consequently (56) becomes

$$R_{22}\Big|_{\theta=\frac{\pi}{2}} = 320 A^3 \frac{x}{y}\left(1 + \frac{\log 4y}{y^2}\right). \tag{57}$$

For $\theta = 0$,

$$X_{22}^{(1)} = 2\alpha_3$$

$$X_{22}^{(2)} = -\alpha_1\alpha_3\left[1 + \frac{k^2}{(R+b)^2}\right] \approx -2\alpha_1\alpha_3$$

$$X_{22}^{(3)} = 0,$$

$$R = 1,$$

so that

$$I = \int_0^{\pi/2} \frac{X_{22}^{(1)} + X_{22}^{(2)} + X_{22}^{(3)}}{R}\, d\phi = -\pi\alpha_1\alpha_3\left(1 - \frac{1}{\alpha_1}\right) \approx -\pi\alpha_1\alpha_3.$$

Hence

$$R_{22}\Big|_{\theta=0} = 160\pi A^3 \frac{x}{y}. \tag{58}$$

From (57) and (58),

$$R_{zz}\big|_{\theta=\pi/2} \Big/ R_{zz}\big|_{\theta=0} = \frac{2}{\pi}\left(1+\frac{1}{y^2}\log 4y\right). \tag{59}$$

Furthermore, from (57) and (50),

$$R_{zz}\big|_{\theta=0} \Big/ R_{FS} = \frac{2}{\pi A}\,\frac{x}{y}. \tag{60}$$

In a typical VLF case, for example,

$$x \approx 4\cdot 10^5$$

$$y \approx 40$$

$$\log y \approx 5$$

$$\frac{x}{y} \approx 10^4 .$$

Consequently, from (59), the radiation resistance of a small loop in the ionosphere varies only a small amount with loop orientations (about 4 db). Furthermore, from (60), the radiation resistance is many orders of magnitude greater than in free space (about $10^4/A$ for the above parameters). For a single-turn loop of 1-meter diameter, $A = 6\pi \cdot 10^{-5}$, so that this factor is about 10^8. From (58), the radiation resistance of this single-turn loop at 18 kc in the above ionosphere is about 10^{-4} ohm. Hence a 10-m diameter single-turn loop would have a radiation resistance of 0.1 ohm, etc.

(58) shows that the radiation resistance of a small loop in the ionosphere varies as A^3, while in free space it varies as A^4. Thus in free space, since $A = k_0 r$, where r is the loop radius, the radiation resistance increases as the fourth power of the radius or of the frequency. In the ionosphere, the radiation resistance increases as the cube of the radius. Since

$$\frac{x}{y} = \frac{\omega_N^2/\omega^2}{\omega_c/\omega} = \frac{\omega_N^2}{\omega\omega_c}$$

it follows from (58) that the radiation resistance in the ionosphere increases only as the square of the frequency in the VLF region.

In view of the favorable radiation properties of a VLF loop for radiation in the ionosphere, it is of interest to calculate the impedance for a practical cross section such as a round wire, instead of the flat strip used in the analysis.

For a single turn loop of radius r , made of round wire of radius a, the inductance is

$$L = 4\pi a \cdot 10^{-9} \log\left(\frac{8r}{a} - 1.75\right)$$

so that its reactance is

$$X_1 = 120\pi A\left(\log\frac{8r}{a} - 1.75\right)$$

where $A = 2\pi r/k_0$.

Calculations will be made for a loop 10 meters in diameter and a frequency of 18 kc. Then

$$A = 2\pi r/k_0 = 6\pi \cdot 10^{-4}.$$

For a wire diameter of 2.5 cm, r/a = 10/0.025 = 400, and

$$X_1 = 4.56 \text{ ohms.}$$

As shown above, the radiation resistance of a 10-m loop at 18 kc is approximately 0.1 ohm. Hence the Q-factor of such a loop is

$$Q = X_1/R \approx 50.$$

The above values of reactance and radiation resistance indicate that a 10-m loop would be easy to feed efficiently. Hence these calculations lead to the conclusion that a properly designed loop can be an efficient antenna for VLF radiation in the ionosphere.

3. NONLINEAR DIAGNOSTICS

There is a profusion of nonlinear effects which can occur in a plasma. These range from harmonic generation and wave interaction to instabilities and the generation of oscillations due to interaction of electromagnetic waves and energetic particle streams. The present studies are aimed at selecting the types of nonlinear effects which can be used to determine basic properties of the plasma, and thus form the basis of diagnostic techniques.

As an initial problem, the combination frequencies set up in a warm plasma by an applied field containing two radio frequencies are being investigated. Since the combination frequency can be selected to bear non-harmonic relation to the applied frequencies, the result can be made substantially independent of instrumental nonlinearities.

3.1 MATHEMATICAL DESCRIPTION OF PLASMA

A plasma is rigorously described by the coupled system of Maxwell's equations plus the Boltzmann equations for the electrons and ions. Instead of the Boltzmann equations, the magnetohydrodynamic (MHD) equations which can be derived from the Boltzmann equations by taking velocity moments can be used. The advantage is that the MHD equations are much easier to handle than the Boltzmann equations.

A plasma is considered in the electron gas approximation in which the positive ions are considered immobile. This approximation is valid if the frequencies of interest are sufficiently high so that the ions do not respond to the fields because of their large mass.

To illustrate the methodology, the MHD-Maxwell equations will be made into a closed system by neglecting thermal effects; i.e., a "cold" plasma is considered. This procedure is followed only at the initial stages of the investigation. The purpose of this is to demonstrate the usefulness of the procedure by using a

relatively simple set of equations. Once this point has been demonstrated, the more complicated equations for the hot plasma can be considered with confidence.

The electron density is written as

$$n = n_0 + n'$$

where n_0 is constant and equal to the ion density. n' is a perturbed density, of zero average value, which is a function of time and space. Similarly, the magnetic field in the medium is decomposed into

$$\underset{\sim}{H} = \underset{\sim}{H}_i + \underset{\sim}{H}_0$$

where $\underset{\sim}{H}_0$ is the external static magnetic field and $\underset{\sim}{H}_i$ is the internal magnetic field due to the moving charges. The equations for the cold plasma then can be put into the following form:

$$\left(\underset{\sim}{\nabla} \times \underset{\sim}{\nabla} \times + \frac{1}{c^2} \frac{\partial^2}{\partial t^2}\right) \underset{\sim}{E} - \frac{n_0 e}{\epsilon_0 c^2} \frac{\partial}{\partial t} \underset{\sim}{v} = F \tag{61}$$

$$\left(\frac{\partial}{\partial t} + \nu\right) \underset{\sim}{v} + \underset{\sim}{v} \times \underset{\sim}{H}_0 + \frac{e}{m} \underset{\sim}{E} = G \tag{62}$$

where:

$$\underset{\sim}{F} \equiv \frac{e}{\epsilon_0 c^2} \frac{\partial}{\partial t} (n' \underset{\sim}{v}) \tag{63}$$

$$\begin{aligned} \underset{\sim}{G} \equiv & -(\underset{\sim}{v} \cdot \underset{\sim}{\nabla}) \underset{\sim}{v} - \frac{n'}{n_0} \left(\frac{\partial}{\partial t} + \underset{\sim}{v} \cdot \underset{\sim}{\nabla}\right) \underset{\sim}{v} \\ & - \frac{e}{m} \underset{\sim}{v} \times \underset{\sim}{H}_i - \frac{n' e}{n_0 m} \left(\underset{\sim}{E} + \underset{\sim}{v} \times \underset{\sim}{H}_i\right) \\ & - \frac{n'}{n_0} \underset{\sim}{v} \times \underset{\sim}{\omega}_c - \frac{n' \nu}{n_0} \underset{\sim}{v} \end{aligned} \tag{64}$$

In (4), $\underset{\sim}{\omega}_c$ is the gyro frequency

$$\underset{\sim}{\omega}_c \equiv \frac{e\mu_0}{m} \underset{\sim}{H}_0 \tag{65}$$

and ν is the collision frequency, which is assumed to be constant.

(61) and (62) have been written so that the linear terms are on the left and the nonlinear terms are on the right.

The basic assumption of the method used is that the nonlinearities are sufficiently small and sufficiently slowly varying in space and time that a perturbation method can be used to solve (61) and (62).

The zero order solutions of (61) and (62) are defined by setting $\underset{\sim}{F} = \underset{\sim}{G} = \underset{\sim}{0}$. Plane wave solutions of the resulting equations can be easily found and are well known. Since the equations are linear, a linear combination of plane waves is also a solution of these equations.

In general, there are three plane wave modes in a cold plasma, two of which propagate, while the third represents a plasma oscillation at the plasma frequency. If finite temperatures are considered, then all three modes propagate.

In view of the above discussion, the zero order field in the plasma is taken to be:

$$\underset{\sim}{E}^{(0)} = \sum_{i=1}^{3} \sum_{j=1}^{2} \left\{ \underset{\sim}{a}_j^{(i)} e^{i(\underset{\sim}{K}_j^{(i)} \cdot \underset{\sim}{x} - \omega_j t)} + \underset{\sim}{a}_j^{(i)} e^{-i(\underset{\sim}{K}_j^{(i)} \cdot \underset{\sim}{x} - \omega_j t)} \right\} \tag{66}$$

where * denotes the complex conjugate. The subscript j labels quantities referring to the two applied frequencies, while the superscript i labels the three plasma modes for each j. The relationship between ω_j and $\underset{\sim}{K}_j^{(i)}$ is determined by solving a well-known algebraic equation. In solving this equation, the polarization of the plasma modes is obtained.

The zero order expressions for $\underset{\sim}{H}_i$, n', and $\underset{\sim}{v}$ are easily found from knowledge of $\underset{\sim}{E}^{(o)}$. By using these expressions in (63) and (64) one can easily compute first approximations $\underset{\sim}{F}^{(o)}$ and $\underset{\sim}{G}^{(o)}$ to $\underset{\sim}{F}$ and $\underset{\sim}{G}$. It is obvious from the forms of (63) and (64) that $\underset{\sim}{F}^{(o)}$ and $\underset{\sim}{G}^{(o)}$ will contain terms with frequencies equal to all combinations of ω_j with j = 1,2.

Using $\underset{\sim}{F}^{(o)}$ and $\underset{\sim}{G}^{(o)}$ in (61) and (62), respectively, first-order equations for $\underset{\sim}{E}$ and $\underset{\sim}{v}$ of the combination frequencies $\omega_1 \pm \omega_2$ can be obtained. The solutions of these equations then give a first-order perturbation solution of the problem. The plasma properties ν and ω_p enter the polarization properties of the waves, so that, for example, a measurement of the relative amplitude and phase by a probe will allow these quantities to be deduced.

This method is being applied to the more interesting problem of a warm plasma which is excited at a sheath. In particular, wave properties which can be measured to deduce electron temperatures will be sought.

REFERENCES

[1] E. Arbel and L. B. Felsen, "Theory of Radiation from Sources in Anisotropic Media, Part I," Symposium on Electromagnetic Theory and Antennas, The Macmillan Company, New York, 1963.

[2] P. C. Clemmow and R. F. Mullaly, "The Dependence of the Refractive Index in Magneto-ionic Theory on the Direction of the Wave Normal," The Physics of the Ionosphere, The Physical Society, London, 1955.

[3] E. Arbel and L. B. Felsen, "Theory of Radiation from Sources in Anisotropic Media, Part II," Electromagnetic Theory and Antennas, E. C. Jordan, Ed., The Macmillan Company, pp. 421-459, 1963.

[4] W. S. Ament, J. C. Katzin, M. Katzin, and B.Y.-C. Koo, "Impedance of a Cylindrical Dipole Having a Sinusoidal Current Distribution in a Homogeneous Anisotropic Ionosphere." Radio Science, v. 68D, pp. 379-405, April 1964.

[5] N. G. de Bruijn, "Asymptotic Methods in Analysis," Interscience Pub. Inc., 1958.

[6] C. Chester, B. Friedman and F. Ursell, "An Extension of the Method of Steepest Descents," Proc. Camb. Phil. Soc., v. 53, pp. 599-611, 1957.

[7] Computation Laboratory, Harvard Univ., "Tables of the Modified Hankel Functions of Order One-third and of Their Derivative," Harvard Univ. Press, 1945.

[8] J. E. Storer, "Impedance of Thin Wire Loop Antennas," Trans. Amer. Inst. Elec. Eng., v. 75, pp. 606-619, 1956.